

NAVAL POSTGRADUATE SCHOOL
Monterey, California

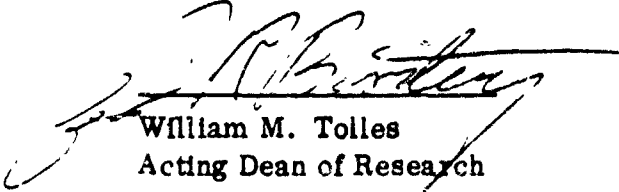
Rear Admiral Isham Linder
Superintendent

Jack R. Borsting
Provost

This thesis prepared in conjunction with research supported in part by Naval Weapons Center, China Lake, California, under project number N6053077WR30252.

Reproduction of all or part of this report is authorized.

Released as a Technical Report by:



William M. Tolles
Acting Dean of Research

UNCLASSIFIED

SECURITY CLASSIFICATION OF THIS PAGE (When Data Entered)

REPORT DOCUMENTATION PAGE		READ INSTRUCTIONS BEFORE COMPLETING FORM
1. REPORT NUMBER NPS61-77-001	2. GOVT ACCESSION NO.	3. RECIPIENT'S CATALOG NUMBER
4. TITLE (and Subtitle) Non-Line-of-Sight Electro-Optic Laser Communications in the Middle Ultraviolet		5. TYPE OF REPORT & PERIOD COVERED Master's Thesis; December 1977
		6. PERFORMING ORG. REPORT NUMBER
7. AUTHOR(s) Dennis Michael Junge in conjunction with William M. Tolles		8. CONTRACT OR GRANT NUMBER(s)
9. PERFORMING ORGANIZATION NAME AND ADDRESS Naval Postgraduate School Monterey, California 93940		10. PROGRAM ELEMENT, PROJECT, TASK AREA & WORK UNIT NUMBERS 62332N; 32342 N6053077WR30252
11. CONTROLLING OFFICE NAME AND ADDRESS Naval Postgraduate School Monterey, California 93940		12. REPORT DATE December 1977
		13. NUMBER OF PAGES 100
14. MONITORING AGENCY NAME & ADDRESS (if different from Controlling Office)		15. SECURITY CLASS. (of this report) Unclassified
		15a. DECLASSIFICATION/DOWNGRADING SCHEDULE
16. DISTRIBUTION STATEMENT (of this Report) Approved for public release; distribution unlimited.		
17. DISTRIBUTION STATEMENT (of the abstract entered in Block 20, if different from Report)		
18. SUPPLEMENTARY NOTES		
19. KEY WORDS (Continue on reverse side if necessary and identify by block number) Electro-optic laser communication middle ultraviolet multiple scattering non-line-of-sight		
20. ABSTRACT (Continue on reverse side if necessary and identify by block number) A Monte Carlo computer simulation was developed to model hypothesized electro-optic laser communication systems operating in the middle ultraviolet region of the spectrum called the solar blind. By assuming various source, propagation, and detector characteristics as well as certain performance parameters it is possible to predict the effective ranges and operating characteristics		

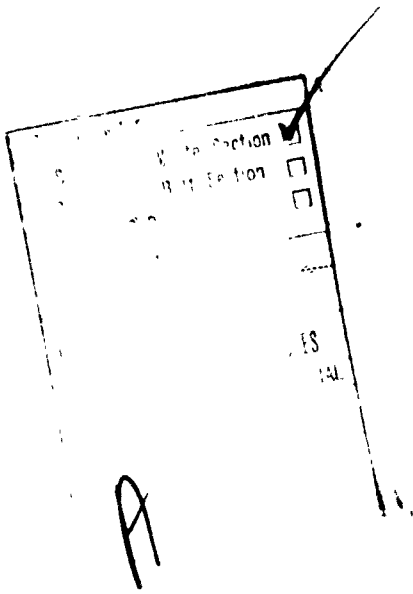
DD FORM 1473
1 JAN 73
(Page 1)EDITION OF 1 NOV 65 IS OBSOLETE
S/N 0102-014-6001

1

UNCLASSIFIED
SECURITY CLASSIFICATION OF THIS PAGE (When Data Entered)

(20. ABSTRACT Continued)

of such a system.



Approved for public release; distribution unlimited.

Non-Line-of-Sight Electro-Optic Laser
Communications in the Middle Ultraviolet

by

Dennis Michael Junge
Lieutenant, United States Navy

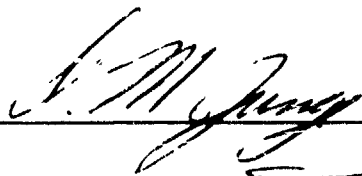
Submitted in partial fulfillment of the
requirements for the degree of

MASTER OF SCIENCE IN APPLIED SCIENCE

from the

NAVAL POSTGRADUATE SCHOOL
December 1977

Author

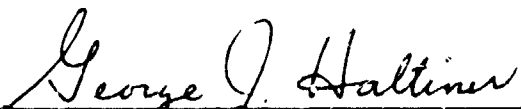


Approved by:


_____ Thesis Advisor


_____ Second Reader


_____ Chairman, Department of Physics and Chemistry


_____ Dean of Science and Engineering

ABSTRACT

A Monte Carlo computer simulation was developed to model hypothesized electro-optic laser communication systems operating in the middle ultraviolet region of the spectrum called the solar blind. By assuming various source, propagation, and detector characteristics as well as certain performance parameters it is possible to predict the effective ranges and operating characteristics of such a system.

ACKNOWLEDGMENTS

The authors would like to express their appreciation to Dr. Michael E. Neer, Aeronautical Research Associates of Princeton (ARAP), Princeton, New Jersey; Dr. Nicholas M. Uros, Pacific Missile Range, Point Mugu, California; and Dr. Alexander S. Zachor, Honeywell, Inc. Radiation Center, Lexington, Massachusetts, for their interest in and contributions to this project.

TABLE OF CONTENTS

I.	INTRODUCTION -----	10
	A. HISTORY -----	10
	B. VISIBLE LIGHT -----	11
	C. INFRARED LIGHT -----	11
	D. ULTRAVIOLET LIGHT -----	12
	E. PURPOSE -----	13
II.	BACKGROUND ----	14
	A. INTRODUCTION -----	14
	B. SOURCES -----	15
	C. PROPAGATION -----	16
	D. DETECTION/DEMODULATION -----	18
III.	STATEMENT OF THE PROBLEM -----	19
IV.	LASER SOURCES -----	21
V.	PROPAGATION PROPERTIES OF THE ATMOSPHERE AND THE MULTIPLE SCATTERING PROBLEM -----	23
	A. INTRODUCTION -----	23
	B. CHARACTERISTICS OF THE ATMOSPHERE -----	23
	1. Attenuation -----	23
	2. Angular Distribution of Scattered Photons -----	24
	C. DESCRIPTION OF THE CHARACTERISTICS OF THE SIMULATION -----	31
	D. CHARACTERISTIC PATTERNS OF MULTIPLY SCATTERED RADIATION -----	32
	E. FIELD OF VIEW CONSIDERATIONS -----	40
	F. PULSE SPREADING CONSIDERATIONS -----	43
	G. SUMMARY -----	46

VI.	SIGNAL-TO-NOISE CONSIDERATIONS -----	47
	A. INTRODUCTION -----	47
	B. FUNDAMENTAL RELATIONSHIPS -----	47
	C. BACKGROUND LEVEL OF RADIATION -----	49
	D. DETECTOR CHARACTERISTICS -----	50
	E. STATISTICAL CONSIDERATIONS -----	51
	F. SUMMARY OF SIGNAL-TO-NOISE CONSIDERATIONS ---	53
VII.	DISCUSSION -----	55
VIII.	CONCLUSIONS -----	58
APPENDIX A:	MONTE CARLO SIMULATION OF THE MULTIPLE SCATTERING PROBLEM -----	59
APPENDIX B:	DEVELOPMENT OF THE FUNDAMENTAL RELATIONSHIP FOR RAYLEIGH SCATTERING -----	68
APPENDIX C:	SAMPLE CALCULATION FOR RANGE PREDICTION --	71
APPENDIX D:	CHECKS ON POSSIBLE ERRORS -----	73
APPENDIX E:	PROGRAM DESCRIPTION AND DOCUMENTATION ----	75
	COMPUTER PROGRAM -----	79
	LIST OF REFERENCES -----	97
	INITIAL DISTRIBUTION LIST -----	100

LIST OF TABLES

TABLE I.	Characteristic Wavelengths of Several Rare Gas-Halide Lasers Along with Some Stokes Shifted Wavelengths Observed with Hydrogen Gas -----	22
TABLE II.	Attenuation Coefficients and Characteristic Ratios for Middle UV Radiation ----	25
TABLE III.	Coefficients Used in the Simulation -----	30
TABLE IV.	Photon Flux Due to Direct and Diffuse Transmittance through the Earth's Atmosphere [12] -----	50
TABLE V.	Photon Flux Required in order to Give a S/N Equal to Ten -----	54
TABLE VI.	Predicted Ranges or Range Bands for Communication in the Middle UV for Pulsed Millijoule Lasers (Simulation) -----	56

LIST OF FIGURES

FIGURE 1	Absolute Phase Function vs. Scattering Angle [23] -----	26
FIGURE 2	Absolute Phase Function vs. Scattering Angle Utilizing a Modified Henyey-Greenstein Function to Approximate the Data by Neer, et al. [23] -----	28
FIGURE 3	Normalized Phase Function vs. Scattering Angle Utilizing a Modified Henyey-Greenstein Function to Approximate the Data by Neer, et al. [23] -----	29
FIGURES 4-7	Photon Scattering Diagram (θ' vs ϕ') as Viewed by a Receiver Located θ Degrees from the Axis of Propagation -----	33
FIGURES 8-10	Contours of Equal Photon Flux as a Function of the Position of the Observer ---	37
FIGURES 11-12	Relative Number of Photons vs Field of View for an Observer Located θ Degrees from the Axis of Propagation -----	41
FIGURES 13-14	Pulse spreading for an Observer Located θ Degrees from the Axis of Propagation -----	44
FIGURE 15	Transmission Characteristics for a Typical Composite Filter -----	52
FIGURE 16	Diagram of the Photon Fixed Coordinate System -----	63

I. INTRODUCTION

A. HISTORY

Historically optical communications systems were developed over line-of-sight paths due to the propagation characteristics of light. In the United States Navy line-of-sight communications became somewhat neglected with the advent of uhf radio technology. For years the only optical communication systems in the navy were the 12 inch (and for a time 24 inch) hand modulated signal lamps, yardarm blinkers, flag hoist, semaphore, and NANCY (a hand modulated infrared system). Some experimentation was conducted in the late 1940's and 1950's using cesium lamps operating in the near infrared (ir) and non-line-of-sight or over-the-horizon (OTH) communication was demonstrated. Interest waned, however, and progress stood still.

Technology has not stood still and today virtually any radio signal can be monitored and the transmitter localized using a direction finding receiver. While communication systems must be reliable and secure, sometimes it is important that they be covert (only detectable by friendly forces). Thus armed with a complete set of radio communication equipment, the unit commander nevertheless may find his forces in EMCON, talking to each other via flashing light.

B. VISIBLE LIGHT

In the 1960's several attempts were again made to demonstrate the feasibility of OTH and over-terrestrial-obstacles communication using atmospheric scattering [1-3]. These efforts utilized visible search lights, flash lamps, and lasers, and communication at night was successfully demonstrated over distances up to fifty kilometers.

Visible radiation is highly attractive because of the low extinction coefficients (depending on weather conditions). Unfortunately it is seriously degraded during daylight hours due to the background radiation from the sun which tends to interfere with detection.

C. INFRARED LIGHT

Recently, efforts have been made to study extended line-of-sight communications utilizing lasers operating in the near ir. One such effort utilized a 1.06 μ laser and employed remotely piloted vehicles (RPVs). Communications at this wavelength appeared quite promising and ranges from 25 to 150 nautical miles have been predicted [4].

In this region of the spectrum, however, there is noticeable background noise due to scattering of incident solar radiation and to emission by atmospheric particles heated by incident radiation. It should be noted that the daylight background visible radiance is due primarily to scattered radiation and night radiance is caused mainly by scattered radiation and moon light. In the near ir daylight

background radiance is due mainly to atmospheric emission, while at night aurora and afterglow are the predominate sources.

D. ULTRAVIOLET LIGHT

There is a portion of the spectrum, however, that has been studied little and may offer much. This is the middle ultraviolet (uv). Atmospheric absorption in the .2 to .3 μ region is caused primarily by ozone [5-6]. The relatively dense layer of ozone (at approximately 22 km) prevents virtually all of the radiation in the 220 to 280 nm region from reaching the surface of the earth. Thus the limiting noise in an electro-optical communication system operating in the middle uv would be self-noise rather than atmospheric noise. Another critical feature to be considered is the attenuation properties of the intervening atmosphere. In the near uv (wavelengths between .3 and .4 μ) the primary attenuation mechanism at low altitude is scattering. This can be divided into Rayleigh scattering and particulate scattering by atmospheric aerosols. Rayleigh scattering, inversely proportional to the fourth power of wavelength, increases quite rapidly as the wavelengths become shorter. In practice, it has been difficult to determine the particulate scattering in the near uv. For clear sky conditions, however, a reasonable estimate of attenuation can be made by assuming that the entire attenuation is due to Rayleigh scattering [2].

In the middle uv particulate scattering is very significant. At high altitudes the large ozone concentration

gives rise to very large absorption coefficients. The concentration of ozone generally decreases as the altitude is decreased. Yet even at sea level the concentration is still high enough to have a significant effect. These propagation characteristics indicate that only short range communication systems operating in the middle uv are likely to be useful. Because of the inherent scattering characteristics of middle uv radiation, along with the minimal background problem in the solar blind region, short range non-line-of-sight communications utilizing broad band light sources have been developed [7-8].

Recently a number of reasonably efficient uv lasers have been developed with energies of .1 to one joule per pulse being reported [9-10]. These represent a new generation of radiation sources to be considered for use in the solar blind. A number of detectors and filters have been available for some time. It was these considerations that led to this study.

E. PURPOSE

The purpose of this effort is to develop an analytical tool for estimating the ranges for which optical communication is possible in the middle uv.

II. BACKGROUND

A. INTRODUCTION

A typical communication system consists of a transmitter, a receiver, and the intervening space between them. The characteristics of the transmitter and the receiver are highly dependent on each other and on the properties of the propagating medium. Each of the components may, however, be treated as a distinct and relatively separate entity. The radiation source, or transmitter, must be suitably modulated to carry information and must have sufficient power to overcome the attenuating mechanisms in the medium in which it operates. The characteristics of the propagating medium are not well defined and in general must be approximated. The detector, or receiver, must have sufficient sensitivity to detect and demodulate the attenuated signal that is embedded in background noise. Each of these components is present in an electro-optical communication system and is discussed below. It will be seen that

- 1) advances in sources dictate a new look at the problem;
- 2) uncertainties in propagation characteristics of the middle uv requires careful experimentation to gather suitable information such that a proposed system may be modeled; and
- 3) certain aspects of detectors, such as filters, critically determine the performance parameters of such a system.

B. SOURCES

Ultraviolet sources suitable for communication purposes include omnidirectional broad band lamps such as xenon or mercury flash lamps, and lasers. Experiments utilizing omnidirectional sources have been carried out for several years at the Aeronautical Research Associates of Princeton (ARAP), Princeton, New Jersey [7-8]. Utilizing a pulsed source at 4810 pps and an average power level of ten to thirty watts, voice communication was demonstrated over a distance of several hundred meters. With suitable modifications, it is estimated that ranges of up to three kilometers may be achieved with the current system. With such a source, the conversion efficiency from input power to output power is about 0.1 percent.

New uv laser sources reported in the last year or so appear to have demonstrated orders of magnitude improvement in efficiency. Utilizing rare gas-halide excimer species, uv output with working efficiencies of up to ten percent are conceivable. Practical working models are already commercially available. Wavelengths in the range of 200 to 400 nm have been reported, indicating that various wavelengths in the middle uv may be attained with these sources. The power output of these devices typically runs from 0.1 joules upwards, depending on the size of the device. The high degree of collimation of the output suggests that the geometric patterns for communication will be highly directional. This is one aspect of the problem which is quite different from that observed for omnidirectional sources.

C. PROPAGATION

The absorption coefficient for middle uv radiation varies by orders of magnitude as a function of wavelength. Scattering by particulates at these wavelengths is more severe than in the visible region of the spectrum. The combined absorption and scattering cross-sections give rise to extinction coefficients which have been measured to be in the range of 0.1 to five per kilometer [11]. Further, variations of an order of magnitude in extinction coefficient over a spectral range of less than fifty nanometers indicates extreme sensitivity to wavelength, due largely to the absorption bands of species such as ozone which appear in this region.

At wavelengths less than 280 nm, the absorption coefficient of atmospheric ozone is sufficiently intense as to eliminate the large majority of solar radiation from the earth's surface [12]. This is largely due to an ozone concentration centered at 20 to 25 km above the surface of the earth. At sea level, the ozone concentration is typically an order of magnitude less than at the higher altitudes. This gives rise to reduced solar background levels without the high extinction coefficients found at higher altitudes. Such behavior suggests that communication in the middle uv may be feasible for relatively short distances at sea level, with a minimum of interference from solar background radiation.

Further major considerations for middle uv propagation are the effects due to multiple scattering. Although the primary light beam may be attenuated by an extinction coefficient which is readily measured, the scattered radiation, especially after multiple scattering, may contribute considerable intensity to the radiation density at an observer. Shettle and Green [12] present calculations for solar flux as a function of the sun's angle with respect to the zenith. Particularly at low angles of incidence, the diffuse radiation is found to be twenty to thirty orders of magnitude more intense than that due to the direct solar radiation. Such figures clearly emphasize the importance of properly treating the effects of multiple scattering when taking into account the effects of particulates in the atmosphere.

In general multiple scattering calculations are cumbersome to handle and yield limited information. Typically these calculations are done on a computer using either an analytical [13] or a Monte Carlo [14-15] approach. The Monte Carlo calculations are relatively easier to model, but utilize a significant amount of computer time and only approximate information is obtained. Some generally useful results have been presented by Bucher [14-15] again indicating orders of magnitude greater radiation densities from the multiple scattering effects than from transmission of direct radiation. The available results from such calculations do not readily answer questions such as 1) what is the

scattering intensity for non-line-of-sight communication given an obstacle with an assumed angle between transmitter-obstacle-receiver; and 2) what is the actual radiation density as a function of field of view and/or position of an observer located off from the axis of propagation at a given distance from a collimated source such as a laser.

D. DETECTION/DEMODULATION

The information available from a pulsed signal depends on the pulse width, repetition rate, and signal-to-noise ratio. Considerations such as these are included in papers by Kennedy [16-17] in which communication through optical scattering channels is discussed. Considerations leading to a suitable signal-to-noise ratio analysis are also presented by Yarif [18] for electro-optical systems. Whether the information is pulsed or continuous wave greatly affects the reception characteristics of the signal. The background light levels coming through the filters utilized before the detector critically determine the signal-to-noise ratio. The characteristics of the filter and detector thus are crucial in determining the information available in a communication system.

III. STATEMENT OF THE PROBLEM

One of the primary constraints on the development and deployment of any new system in the United States Navy is the limited fiscal resources available for such efforts. With the advent of new technology it is nevertheless impossible to utilize the technology to build a new system without first having a mission or demonstrated need for that system and second having a well-defined degree of confidence in the ability of that system to meet that need.

An electro-optical communication system utilizing a laser operating in the middle uv is such a system. (It requires little or no imagination to visualize the advantages of rapid short range, possibly non-line-of-sight, optical communications over the methods presently employed by the Fleet.) While it is beyond the scope of this project to develop such a system, it is within the scope of this effort to formulate a model of such a system capable of predicting the various parameters of that system.

The need for modeling is further enhanced by the limited amount of information available concerning the middle uv. By utilizing available information and by characterizing source, propagation, filter and detector characteristics, it is possible to formulate a model that will yield order of magnitude results for any proposed system. In the process of modeling and analysis the need for critical experiments

which would allow the modeling efforts to proceed with a greater degree of accuracy is sure to be revealed.

IV. LASER SOURCES

The past two or three years have seen a rapid development of lasers operating in the ultraviolet. The most notable recent advances have occurred with the rare gas-halide lasers in which an excited state eximer is formed. With species such as XeF^* , the ground state is not an associated molecule, thus depopulation of the lower level is not a barrier to population inversion. Further, such rare gas-halide lasers have an inherently high quantum efficiency. Efficiencies relative to the energy deposited by an excitation electron beam are as high as ten percent, while overall working efficiencies of up to one percent have been reported [9,10,19]. With higher overall efficiencies anticipated, such lasers represent an attractive source of radiation for middle uv applications.

The observed wavelengths of several rare gas-halide lasers are presented in Table I. It should be noted that the laser output from these sources may be Raman shifted with reasonable high conversion efficiencies [20]. By passing the output from a KrF laser through ten atmospheres of hydrogen, conversion to the first stokes wavelength of 25 percent and to the second stokes wavelength of ten percent was observed [20]. At eighty atmospheres pressure, more than fifty percent conversion efficiency to the first stokes wavelength has been observed.

TABLE I

Characteristic Wavelengths of Several Rare
Gas-Halide Lasers Along with Some Stokes
Shifted Wavelengths Observed with Hydrogen Gas

<u>Eximer</u>	<u>Wavelength (nm)</u>	<u>First Stokes Wavelength (nm)</u>	<u>Second Stokes Wavelength (nm)</u>
KrF	249	279	318
XeF	351		
XeCl	308		
XeBr	282	322	

The practical performance of rare gas-halide lasers is illustrated by the commercial availability of a model which will produce 0.1 joule pulses at 15 pps. One table top model is reported to produce 1.5 joule pulses with a 125 nanosecond pulse width. The development of these lasers is in its infancy. Sources with higher repetition rates and greater reliability are to be expected.

Due to the rapidly expanding availability of middle uv lasers sources, no single presently available source is assumed, but rather the effort in the succeeding sections considers the possibility of utilizing a middle uv source at representative wavelengths and with an output power consisting of millijoule to joule pulses. Thus the behavior of any unforeseen laser or coherent beam may be predicted.

V. PROPAGATION PROPERTIES OF THE ATMOSPHERE AND THE MULTIPLE SCATTERING PROBLEM

A. INTRODUCTION

A laser signal propagating through the atmosphere is subjected to various attenuation mechanisms. The time spread of a pulse can be broadened due to scattering, while the amplitude can be decreased due to absorption and scattering by atmospheric constituents. The inherent directionality of a laser source indicates that the position of the detector relative to the source should also affect the reception of the signal. Since a large fraction of the total extinction process is due to scattering, multiple scattering should be an important consideration affecting the propagation characteristics for distances greater than one or two extinction lengths.

A complete description of all of the effects of the atmosphere including inhomogeneities (clouds, terrestrial objects, surface effects, etc.) is beyond the scope of this paper. A relatively concise treatment of the atmosphere and the multiple scattering problem entails characterizing the atmosphere, simulating atmospheric effects, and tabulating the results of the simulation.

B. CHARACTERISTICS OF THE ATMOSPHERE

1. Attenuation

In order to characterize the propagation of optical information in the atmosphere it was first necessary to

determine the extinction, absorption, and scattering coefficients. Table II was constructed based primarily on the information reported by Dunkelman [21]. The Rayleigh scattering coefficients were adapted from Penndorf [22].

For the purpose of this investigation the following definitions and relationships apply:

λ is the wavelength

K_A is the absorption coefficient

K_{SR} is the Rayleigh scattering coefficient

K_{SP} is the particulate scattering coefficient

K_S is the total scattering coefficient

K is the total extinction coefficient

$$K_S = K_{SR} + K_{SP}$$

$$K = K_S + K_A$$

R_S is the ratio of K_S to K or (K_S/K)

R_P is the ratio of K_{SP} to K_S or (K_{SP}/K_S)

From Table II it can be seen that K_A , K_{SR} , and K tend to decrease as wavelength increases in the middle uv. The relationship of K_{SP} and consequently K_S , R_S , and R_P to wavelength is not so easily described.

2. Angular Distribution of Scattered Photons

Complete characterization of the propagation of optical information required the angular distribution or phase function, $P(\theta)$, of the scattered photons for the wavelengths of interest. Figure 1 [23] was the primary source for phase function information.

TABLE II
Attenuation Coefficients and Characteristic Ratios
for Middle uv Radiation

λ (nm)	K_A (km^{-1})	K_{SR} (km^{-1})	K_{SP} (km^{-1})	K_S (km^{-1})	K (km^{-1})	R_S (K_S/K)	R_P (K_{SP}/K_S)
230	2.58-3.5	.4934	.03-2.9	.52-3.4	3.1-6.0	.17-.57	.06-.85
240	1.43-2.8	.4061	.26-3.2	.67-3.6	2.1-5.0	.32-.72	.39-.89
250	.68-2.6	.3382	.18-2.4	.52-2.7	1.2-3.4	.43-.79	.35-.89
260	.43-2.4	.2842	.29-2.2	.57-2.5	1.0-2.9	.57-.86	.51-.88
270	.23-1.6	.2404	.33-2.1	.57-2.3	.80-2.6	.71-.88	.58-.91
280	.13-.89	.2055	.065-1.9	.27-2.1	.40-2.2	.68-.95	.24-.90
290	.046-.32	.1765	.078-1.9	.25-2.1	.30-2.1	.83-1.00	.31-.90
300	.012-.081	.1525	.056-1.7	.21-1.9	.22-1.9	.95-1.00	.27-.89
310	.003-.021	.1326	.044-1.6	.17-1.7	.18-1.8	.94	.26-.94

ABSOLUTE PHASE FUNCTION
vs SCATTERING ANGLE

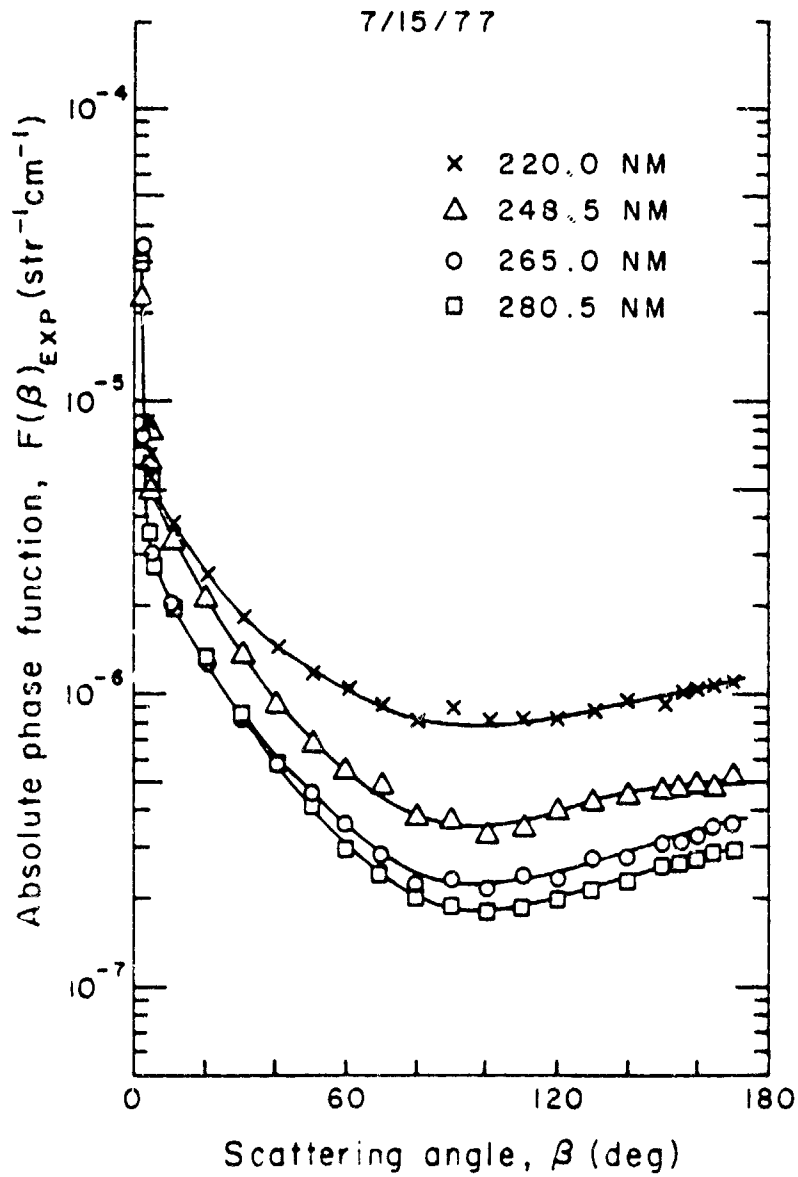


FIGURE 1. Absolute Phase Function vs. Scattering Angle [23]

In order to mathematically model this information, the Henyey-Greenstein function, Eq. 1, and some of its modifications were studied. The Neer-Sandri function [7], Eq. 2, was a logical choice; however, the function used by Zachor [24], Eq. 3, was chosen for simplicity in modifying the author's initial phase function to properly account for backscattering.

$$P(\theta, g) = \frac{1-g^2}{4\pi} \left[\frac{1}{(1+g^2-2g \cos \theta)^{3/2}} \right] \quad (1)$$

$$P(\theta, g) = \frac{1-g^2}{4\pi} \left[\frac{1}{(1+g^2-2g \cos \theta)^{3/2}} + \frac{g(3 \cos^2 \theta - 1)}{2 |\cos \theta_0| (1+g^2-2g |\cos \theta_0|)^{3/2}} \right] \quad (2)$$

$$\text{where } |\cos \theta_0| = 1/7$$

$$P(\theta, g) = \frac{1-g^2}{4\pi} \left[\frac{1}{(1+g^2-2g \cos \theta)^{3/2}} + \frac{f \cdot 0.5(3 \cos^2 \theta - 1)}{(1+g^2)^{3/2}} \right] \quad (3)$$

Fitting the data reported by Neer [23] with Eq. 3 resulted in Figures 2 and 3. These figures represent the absolute and normalized phase functions, while Table III lists the coefficients, utilized for this simulation.

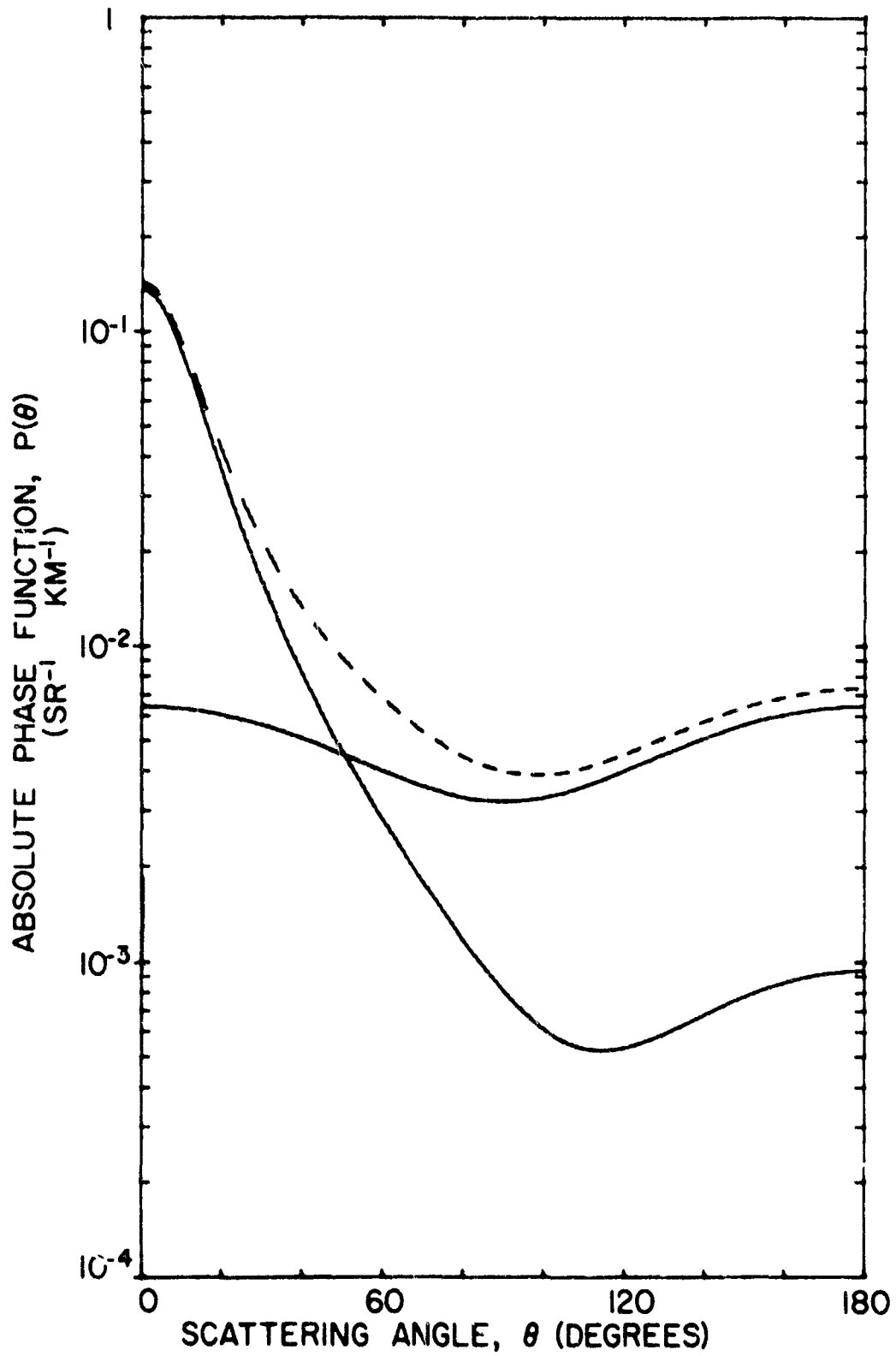


FIGURE 2. Absolute Phase Function vs. Scattering Angle Utilizing a Modified Henyey-Greenstein Function to Approximate the Data by Neer, et al. [23]

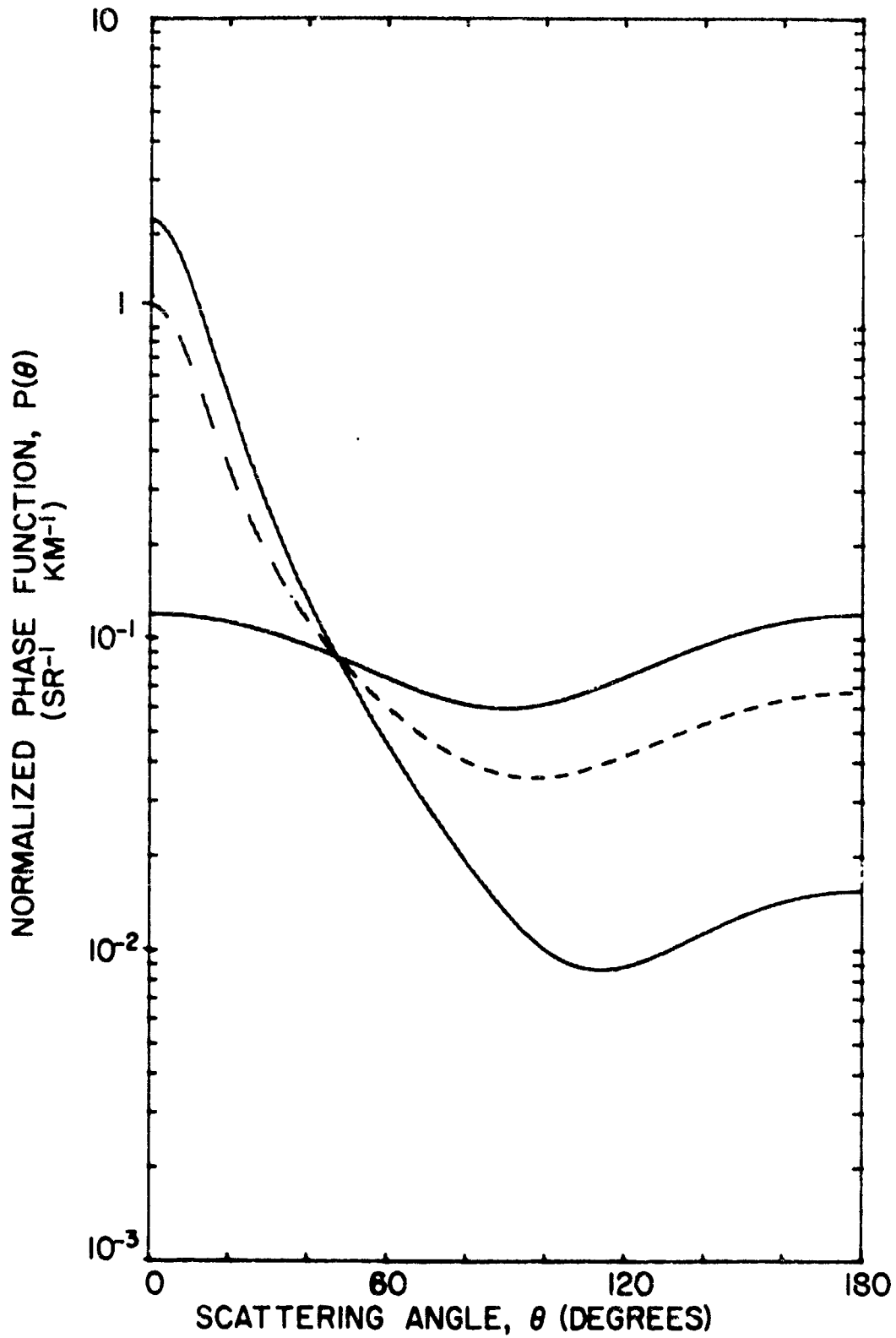


FIGURE 3. Normalized Phase Function vs. Scattering Angle Utilizing a Modified Henyey-Greenstein Function to Approximate the Data by Neer, et al. [23]

TABLE III
Coefficients Used in the Simulation

λ (nm)	K_A (km^{-1})	K_{SR} (km^{-1})	K_{SP} (km^{-1})	K_S (km^{-1})	K (km^{-1})	R_S (K_S/K)	R_P (K_{SP}/K_S)
250	.9372	.3382	.7187	1.0569	1.9941	.53	.68
280	.2185	.2055	.6165	.8220	1.0405	.79	.75
300	.0289	.1525	.5407	.6932	.7221	.96	.78

For all three cases the values of g and f utilized were 0.75 and 0.5, respectively. The values for 250 nm appear to be optimistic while the values for 300 nm appear to be somewhat pessimistic.

C. DESCRIPTION OF THE CHARACTERISTICS OF THE SIMULATION

The purpose of this simulation was to provide approximate results for the multiple scattering problem. By assuming various source, propagation, and detector characteristics, a user could in principle predict the effectiveness of a proposed system.

The Monte Carlo method described in Appendix A was employed to generate information detailing characteristic patterns of photon scattering as a function of wavelength, position of an observer, pulse spreading, and field of view of the detector being employed. The observer may be located at any arbitrary angle off from the axis of propagation and at any arbitrary distance from the source (measured in extinction lengths).

Of primary interest were the characteristic patterns of multiply scattered radiation. The simulation provided for obtaining diagrams of photon flux at a given position as viewed by either the source or the receiver. In addition, the patterns received by the detector were capable of being limited by field of view restrictions. By measuring the photon flux at a given position, contours of equal photon flux were generated. These contours provided a simple means of visualizing the radiation patterns.

Detector field of view considerations indicate the field of view required to receive a given threshold of photons at a fixed position as well as the maximum range at a given angle that a threshold number of photons can be

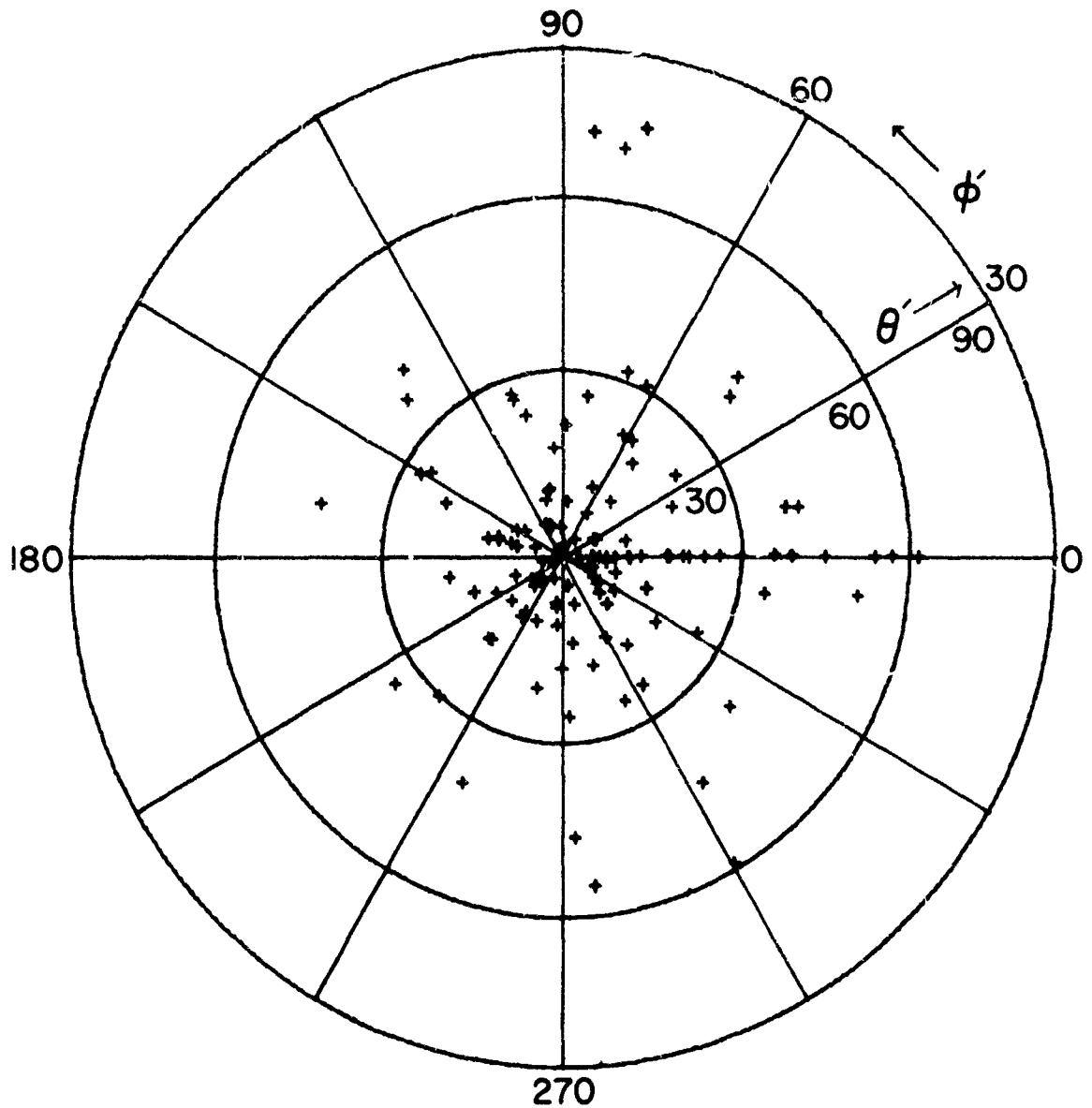
detected for a fixed field of view. Finally, pulse spreading information due to the time delay caused by multiple scattering was also available.

D. CHARACTERISTIC PATTERNS OF MULTIPLY SCATTERED RADIATION

Figures 4 and 5 represent the pattern of photons received by a 180 degree field of view detector located zero to nine and 36 to 45 degrees off from the axis of propagation respectively at one extinction length from a 300 nm laser source. As the detector approached the axis of propagation more photons were received. The photons along the ϕ prime equal to zero axis represent single scattered radiation. Many of the photons received were, however, multiply scattered.

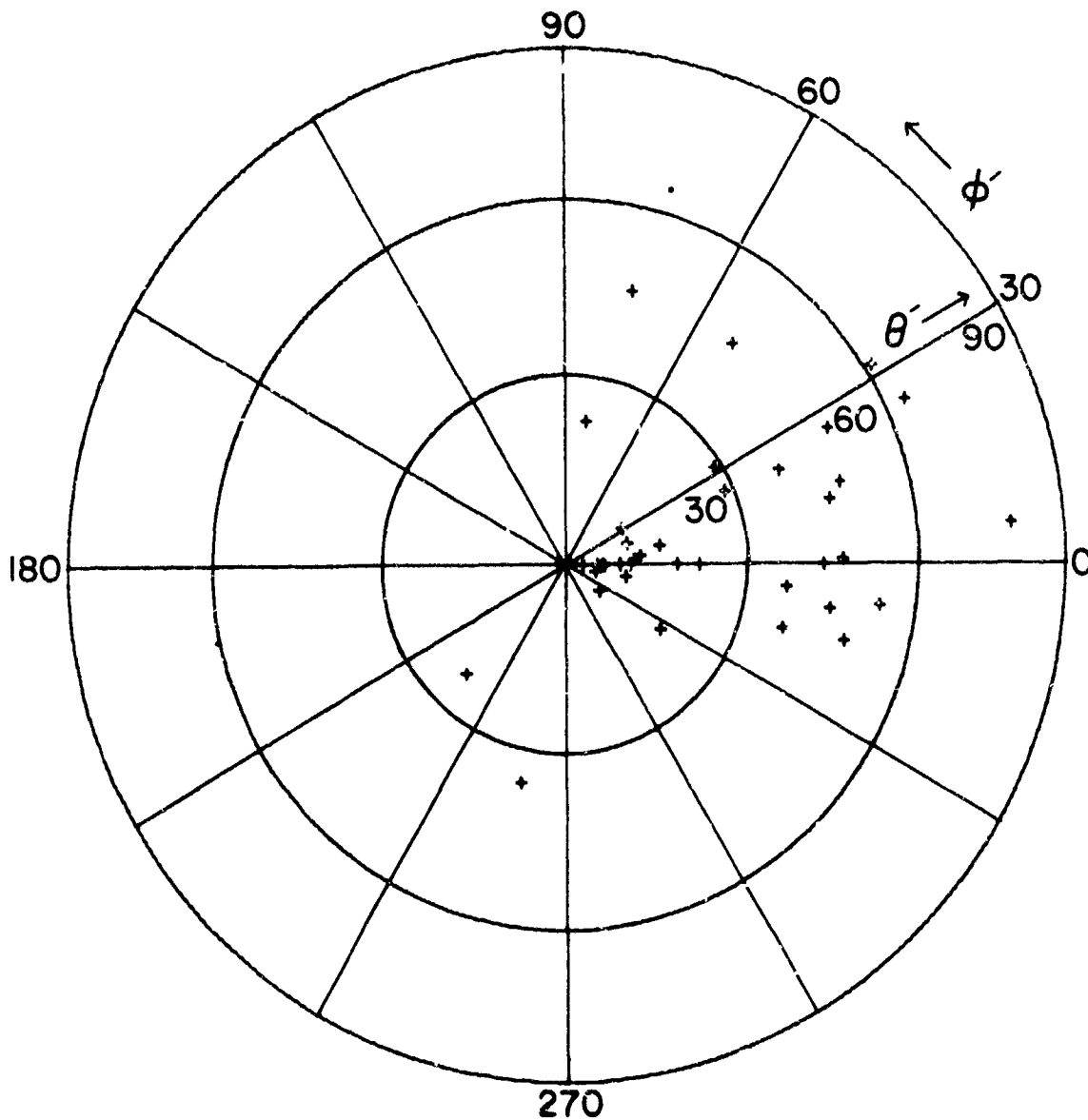
Figures 4 and 5 are similar to Figures 6 and 7 only in the latter figures the receiver is located five extinction lengths from the source. The percentages of multiply scattered photons increases greatly as the receiver is moved either off from the axis of propagation or away from the source. At five extinction lengths, virtually none of the radiation received is single scattered. This is a strong indication of the hazards of single scattering models in the middle uv.

Figures 8, 9, and 10 represent the contours of equal photon flux for 250, 280, and 300 nm wavelengths. The label for each contour is



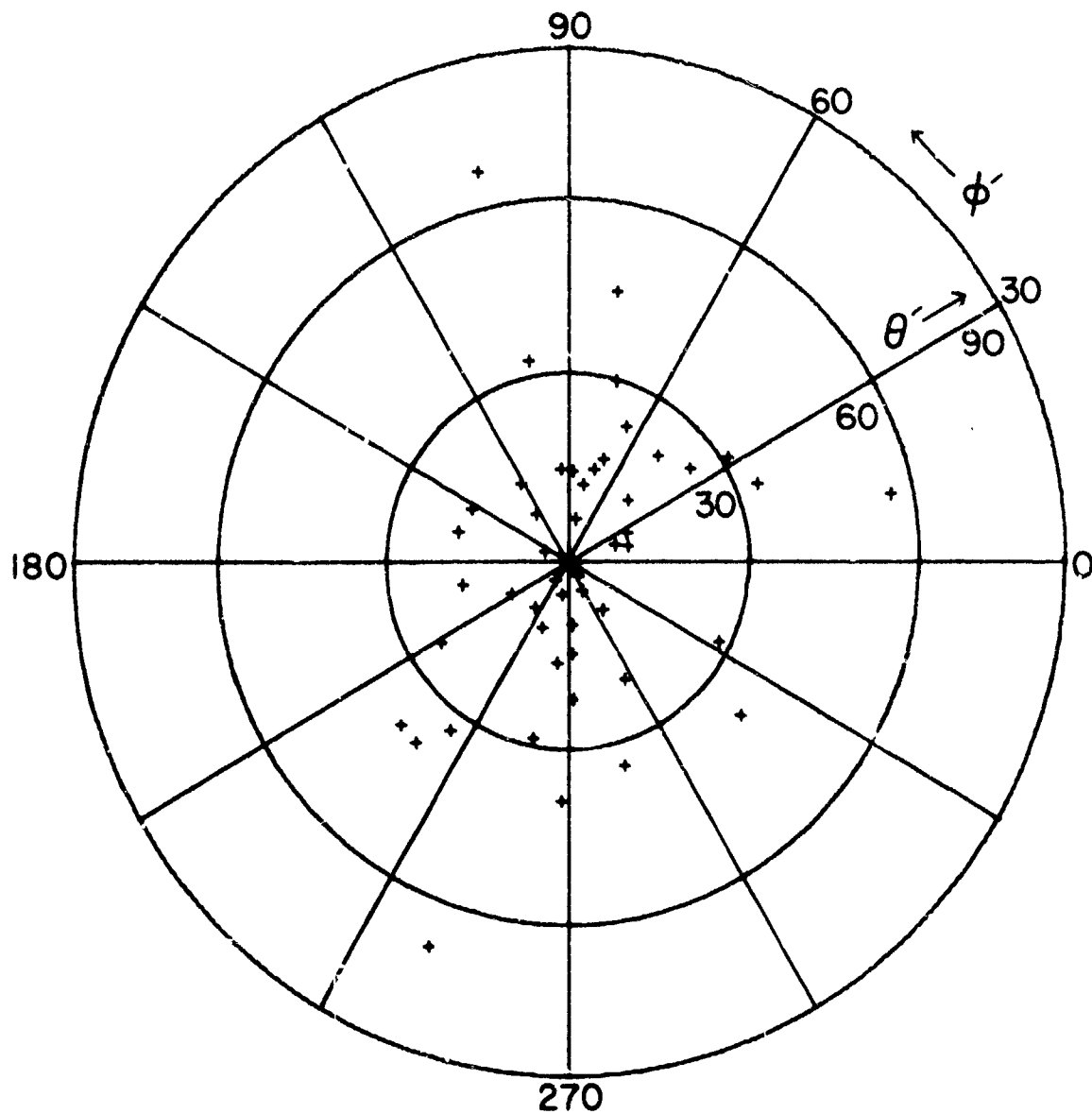
270
 RECEIVER LOCATED ONE EXTINCTION LENGTH
 FROM THE SOURCE. $\theta = 0$ TO 9 DEGREES
 $\lambda = 300$ NM. FIELD OF VIEW = 180 DEGREES

FIGURE 4. Photon Scattering Diagram (θ' vs ϕ') as Viewed by a Receiver Located θ Degrees from the Axis of Propagation.



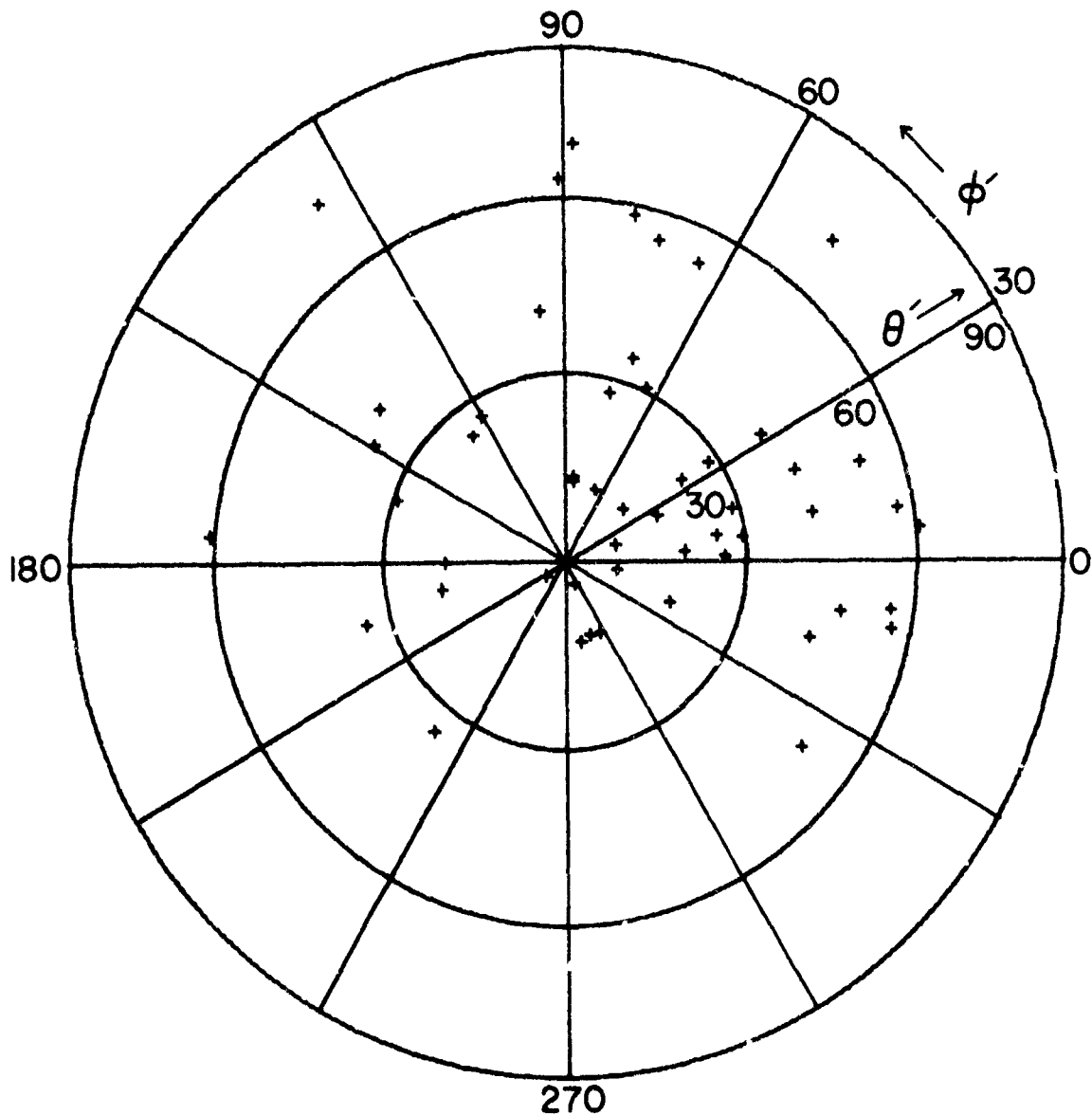
RECEIVER LOCATED ONE EXTINCTION LENGTH
 FROM THE SOURCE. $\theta = 36$ TO 45 DEGREES
 $\lambda = 300$ NM. FIELD OF VIEW = 180 DEGREES

FIGURE 5. Photon Scattering Diagram (θ' vs ϕ') as Viewed by a Receiver Located θ Degrees from the Axis of Propagation.



270
 RECEIVER LOCATED FIVE EXTINCTION LENGTHS
 FROM THE SOURCE. $\theta = 0$ TO 9 DEGREES
 $\lambda = 300$ NM. FIELD OF VIEW = 180 DEGREES

FIGURE 6. Photon Scattering Diagram (θ' vs ϕ') as Viewed by a Receiver Located θ Degrees from the Axis of Propagation



RECEIVER LOCATED FIVE EXTINCTION LENGTHS
 FROM THE SOURCE. $\theta = 36$ TO 45 DEGREES
 $\lambda = 300$ NM. FIELD OF VIEW = 180 DEGREES

FIGURE 7. Photon Scattering Diagram (θ' vs ϕ') as Viewed
 by a Receiver Located θ Degrees from the Axis
 of Propagation

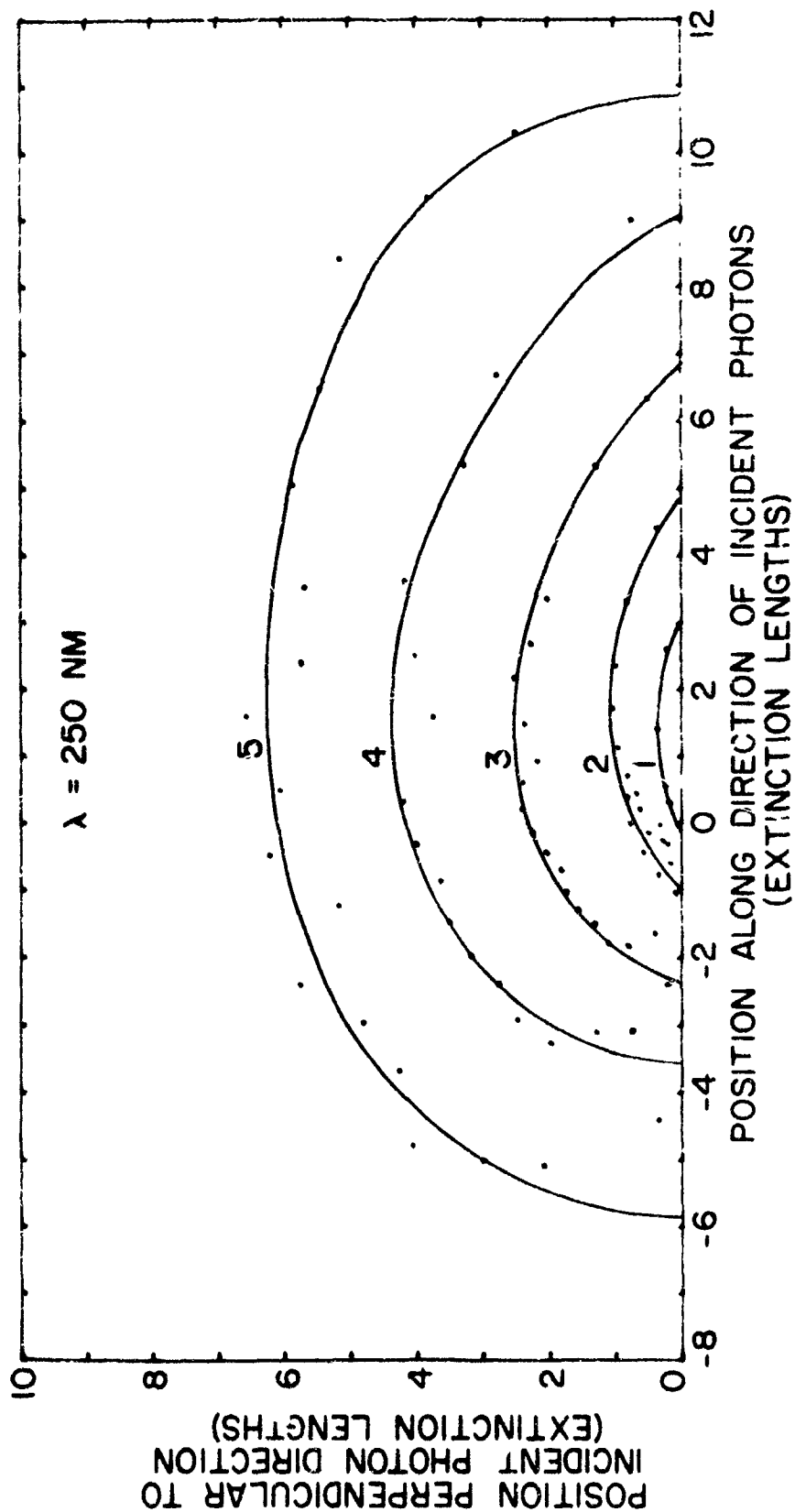


FIGURE 8. Contours of Equal Photon Flux as a Function of the Position of the Observer

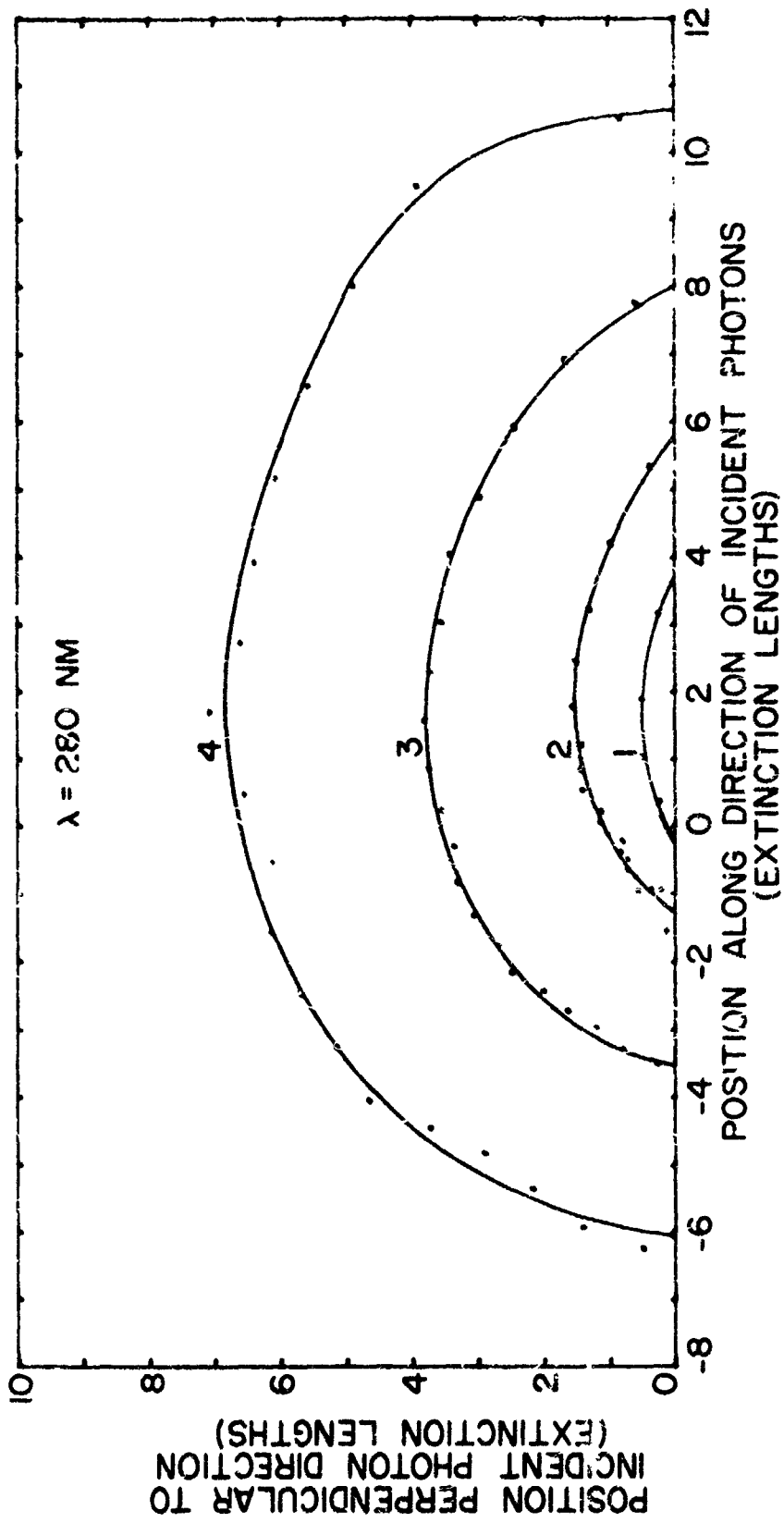


FIGURE 9. Contours of Equal Photon Flux as a Function of the Position of the Observer

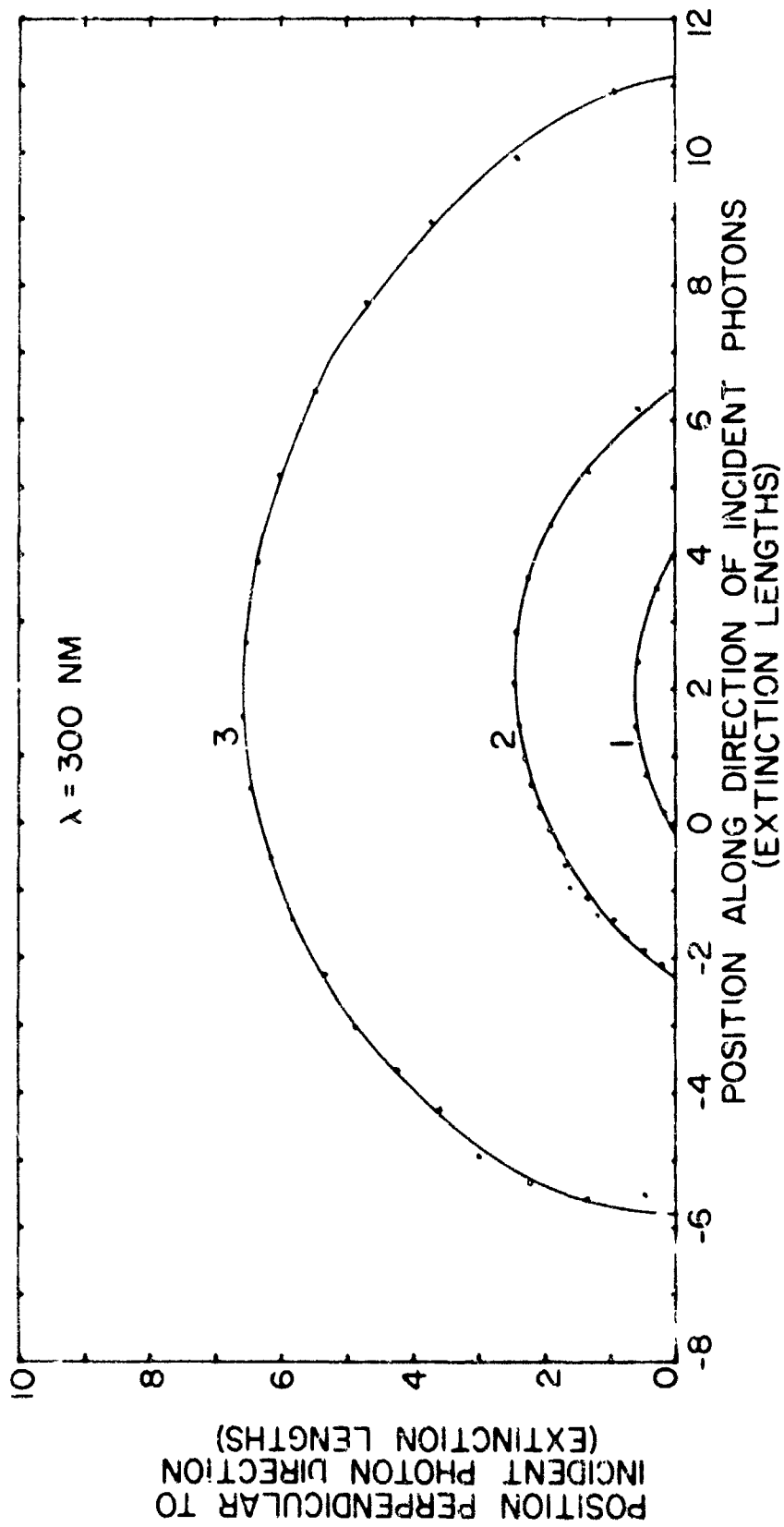


FIGURE 10. Contours of Equal Photon Flux as a Function of the Position of the Observer

$$\text{Relative Flux} = -\log_{10} \left[\frac{N}{N_0 2\pi R^2 (\cos\theta_1 - \cos\theta_2)} \right]$$

(4)

where $2\pi R^2 (\cos\theta_1 - \cos\theta_2)$ is the area of that portion of a hemisphere located R extinction lengths from the source subtended by θ_1 and θ_2 , N is the number of photons penetrating that area, and N_0 is the number of photons leaving the source. Each successive contour of photon flux represents a decrease of one order of magnitude in the relative photon flux. Thus, for example, the contour labeled 2 gives the location at which the photon flux is 10^{-2} photons per unit area, where unit area is one extinction length squared.

E. FIELD OF VIEW CONSIDERATIONS

Figures 11 and 12 represent the relative number of photons detected at a receiver located zero to nine and 36 to 45 degrees off from the axis of propagation at one and five extinction lengths respectively from a 250 nm laser source. A sixty degree (full cone angle) field of view detector would receive seventy-five to eighty percent of the incident radiation for the θ_1 (zero to nine degrees) and the θ_2 (36 to 45 degrees) cases at one extinction length. At five extinction lengths these percentages tend to remain stable. Thus, given a minimum required photon flux at a detector, it is possible to select the proper field of view for that detector. Conversely, utilizing a fixed

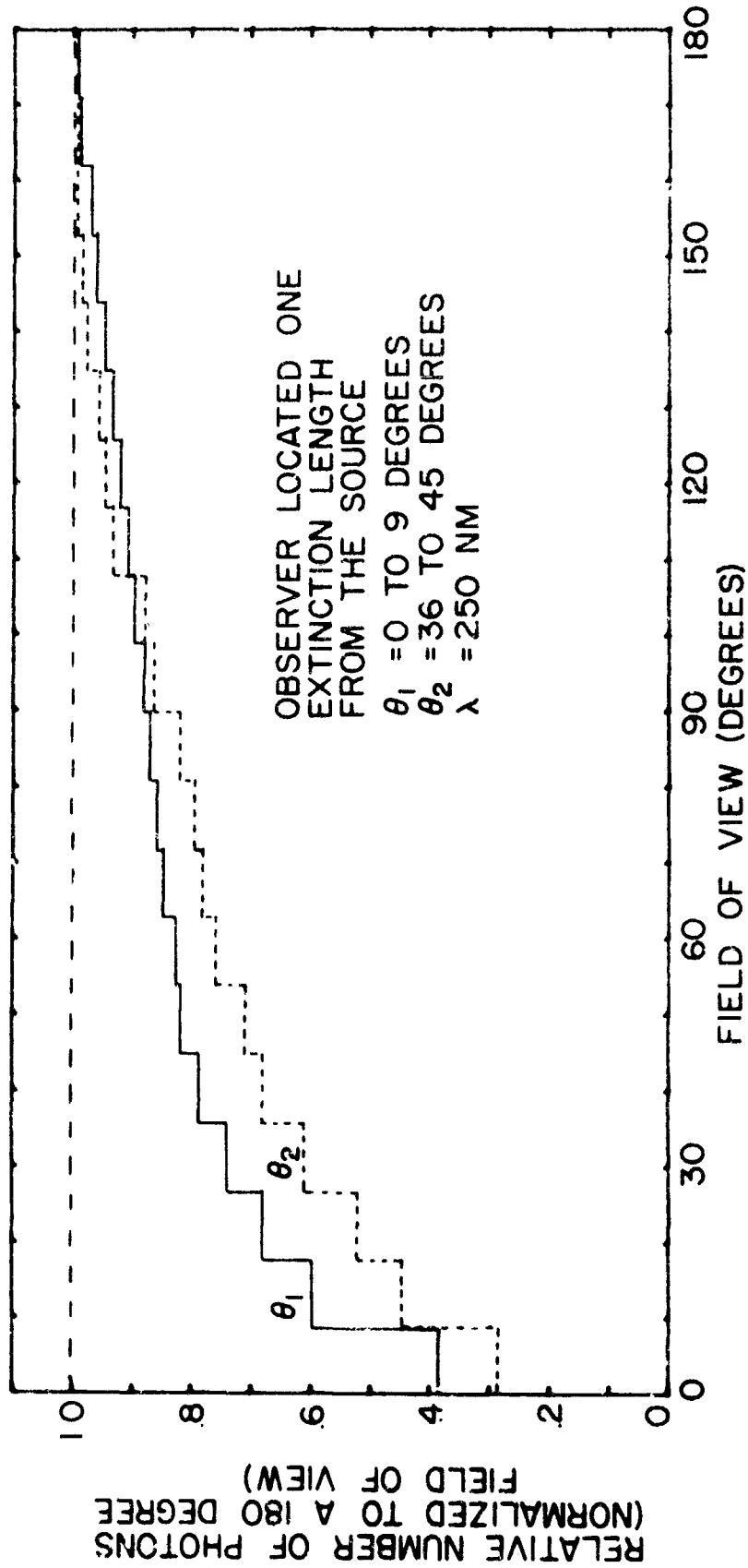


FIGURE 11. Relative Number of Photons vs Field of View for an Observer Located θ Degrees from the Axis of Propagation

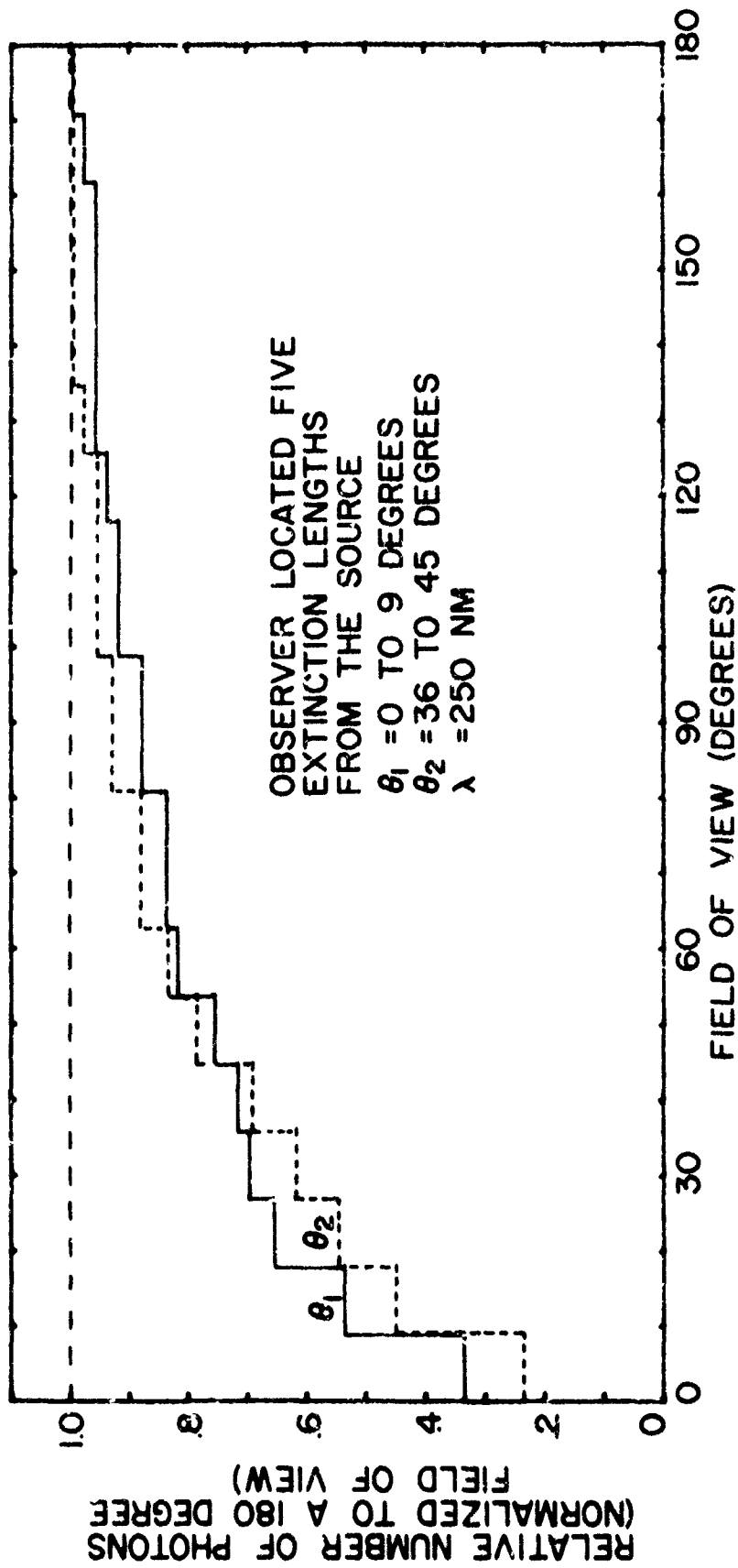


FIGURE 12. Relative Number of Photons vs Field of View for an Observer Located 6 Degrees from the Axis of Propagation

field of view detector, it is possible to determine the maximum effective range for a minimum photon flux. (The results for 280 and 300 nm were substantially the same as the 250 nm simulation).

F. PULSE SPREADING CONSIDERATIONS

Figures 13 and 14 represent the pulse spreading as received by a detector located zero to nine and 36 to 45 degrees off from the axis of propagation at one and five extinction lengths from a 250 nm laser source, respectively. The pulse spreading function is a function of the position of the observer and time dispersion caused by multiple scattering. The relative time dispersion, $T(R,D)$ is defined as follows:

$$T(R,D) = \frac{D}{R} - 1 \quad (5)$$

where D is the total distance traveled by each photon and R is the distance from the source to the shell penetrated by each photon.

The results of pulse spreading at other distances and angles was examined. The pulse spreading function is nearly constant for values of R from one to ten extinction lengths, thus one figure suffices as an approximation to any distance in this angular range. The increase in pulse spreading with increasing angle is illustrated with one additional plot at 36 to 45 degrees off from the

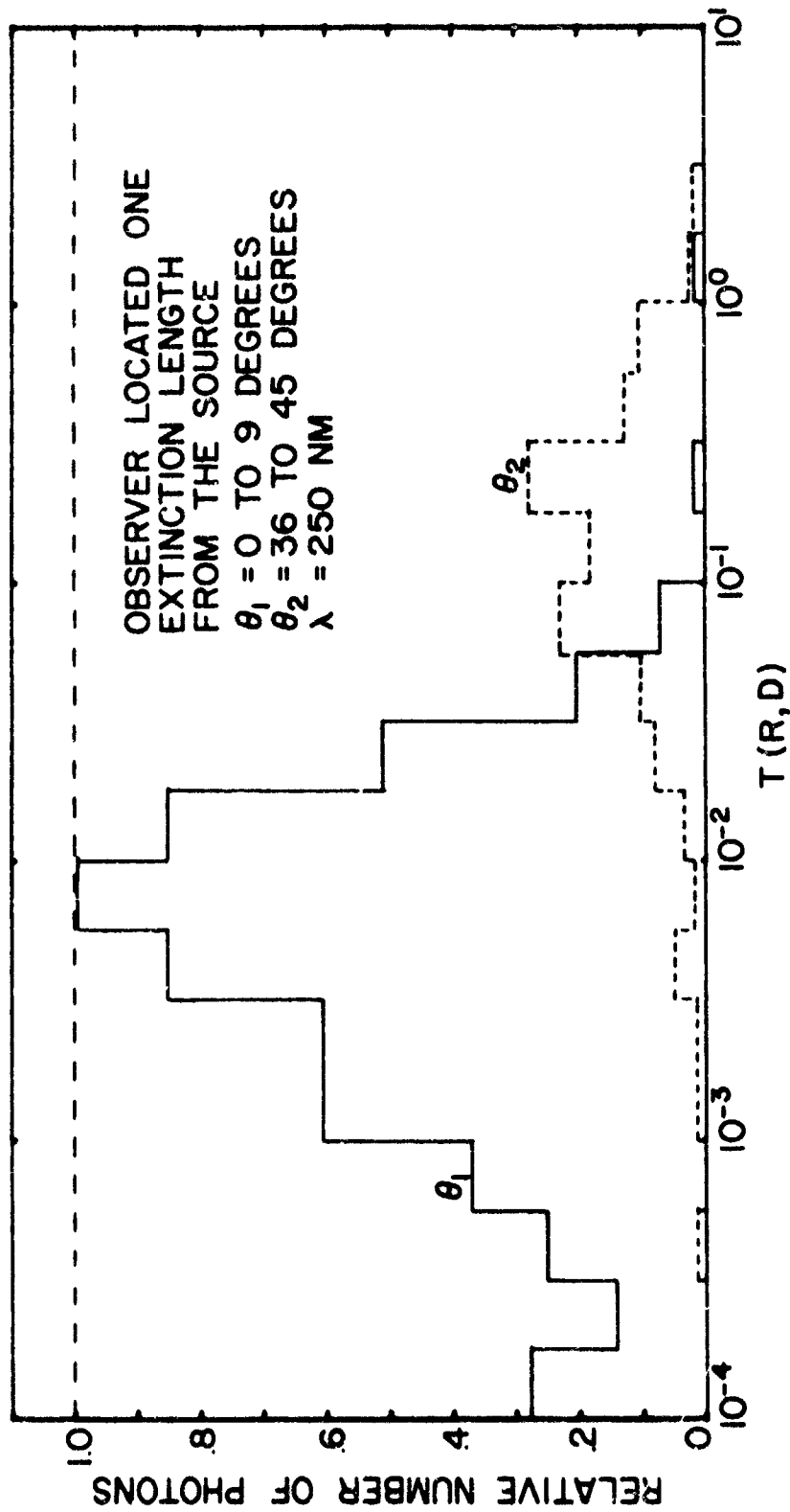


FIGURE 13. Pulse Spreading for an Observer Located θ Degrees from the Axis of Propagation

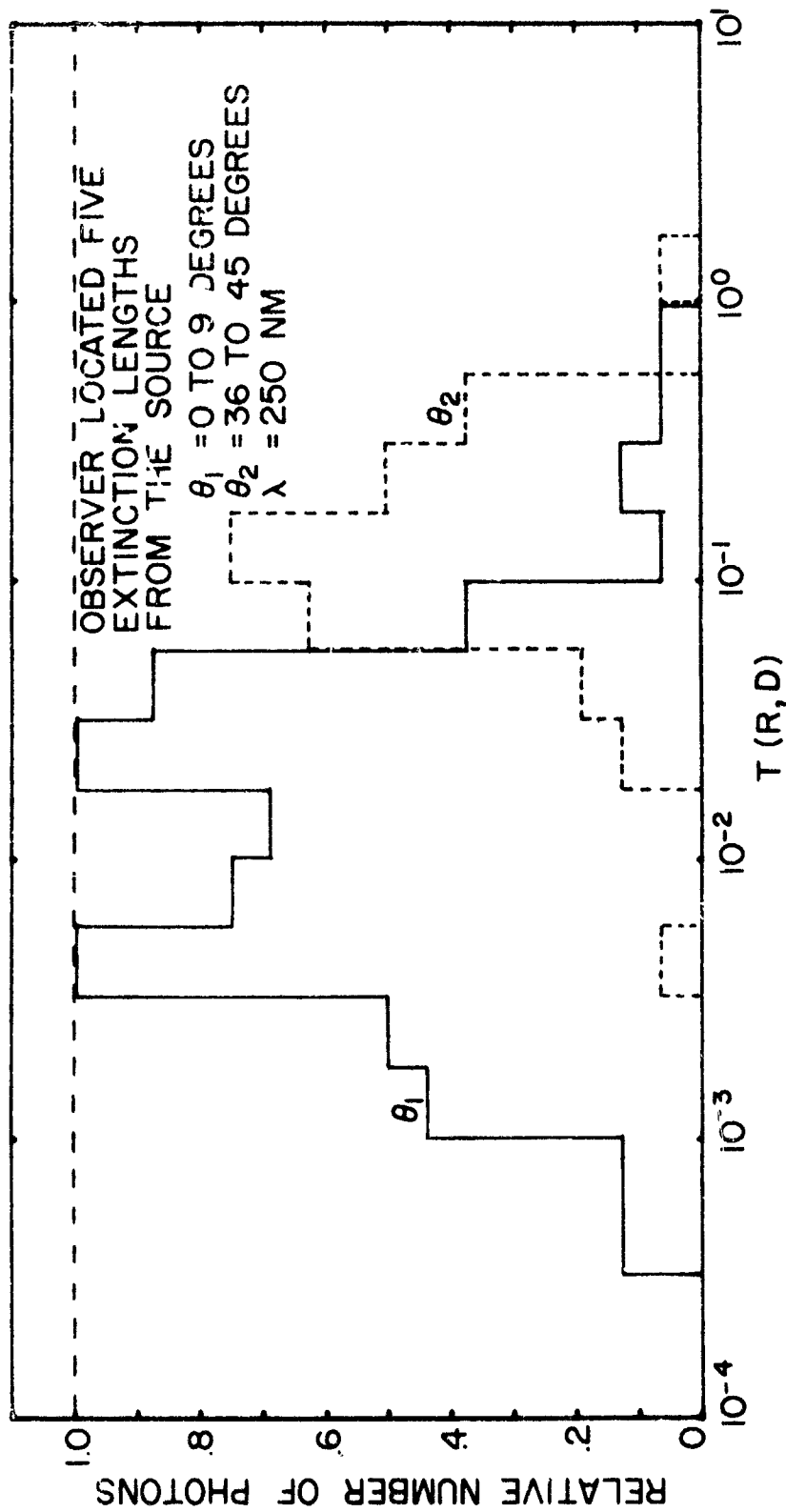


FIGURE 14. Pulse Spreading for an Observer Located Degrees from the Axis of Propagation

axis of propagation. Reproduction of the results at each cone angle introduces a cumbersome presentation of this information, hence only one representative sample is included.

G. SUMMARY

The absorption and scattering coefficients as well as the phase functions from previous experiments were utilized and the behavior of multiple scattered radiation was simulated using the Monte Carlo method. This model was used to study the characteristics of the source beam at a receiver located an arbitrary angle off from the axis of propagation at a given distance from the source. With such information available, the geometric pattern of possible communication links can be determined. A photon density as a function of receiver field of view and position of the observer was determined as well as the effects of multiple scattering on pulse spreading.

VI. SIGNAL-TO-NOISE CONSIDERATIONS

A. INTRODUCTION

The photon flux information presented in the previous section may be utilized to estimate the signal-to-noise ratio (S/N or SNR). This information, however, must be used in conjunction with the characteristics of the detector. Additional considerations therefore include the characteristics of the optical filter, quantum efficiency of the detector, background level of radiation, etc. This section considers the characteristics of available devices and of known atmospheric flux levels in order to estimate the flux level necessary for reliable communication.

B. FUNDAMENTAL RELATIONSHIPS

The detector current generated by a light signal of power P_S and of frequency ν is

$$i_S = \frac{GneP_S}{h\nu} \quad (6)$$

where G is the gain of the detector, η is the quantum efficiency of the detector, e is the electronic charge, and h is Planck's constant [18].

The dominant noise mechanism for detectors operating in the visible and ultraviolet region of the spectrum is shot noise. The mean square of the noise current due to this noise mechanism is

$$\langle i_n^2 \rangle = 2eG^2 [i_d + \frac{\eta e}{h\nu} (P_S + P_B)] B \quad (7)$$

where G is the gain of the detection device (typically a photomultiplier), i_d is the dark current, P_B is the power of the background radiation present due to sources other than that from the desired signal, and B is the bandwidth of the receiver [18, 25, 26, 27].

The desired expression for S/N is thus the ratio of the square of Equations (6) and of (7).

$$S/N = \frac{\langle i_s^2 \rangle}{\langle i_n^2 \rangle} = \frac{\left(\frac{\eta e P_S}{h\nu}\right)^2}{2e [i_d + \frac{\eta e}{h\nu} (P_S + P_B)] B} \quad (8)$$

In several specific cases the dark current i_d is negligible, whereupon Equation (8) reduces to Equation (9).

$$S/N \approx \frac{\eta P_S}{2h\nu B} \left(\frac{P_S}{P_S + P_B}\right) \quad (9)$$

For pulsed signals having a time duration of τ , the bandwidth B is effectively $1/2\tau$. The relationship for S/N thus reduces to the number of photons converted to electrons in a pulse, degraded by the ratio of the signal power to total power received over the duration of the pulse.

Each of the expressions for S/N may be modified slightly by consideration of a duty factor, introduced to account for the fact that a signal is not constant over the duration

of a pulse. Consideration of this introduces a multiplicative factor equal to Equation (10).

$$\frac{D_S}{D_N} = \frac{\int_{-\tau/2}^{\tau/2} \left(\frac{i_S(t)}{i_S(0)} \right)^2 dt}{\int_{-\tau/2}^{\tau/2} \left(\frac{i_N(t)}{i_N(0)} \right)^2 dt} \quad (10)$$

where D_S/D_N is the ratio of the duty factor of the signal to that of the noise over the duration of the pulse, τ .

C. BACKGROUND LEVELS OF RADIATION

The expressions for S/N involve critically the background levels of radiation due to other sources. In communication experiments this is typically due to scattered sunlight. Reliable flux levels at wavelengths longer than 300 nm are reported by Valley [28]. The flux levels at shorter wavelengths are a result of both direct and diffuse transmission. These levels are critically dependent on the thickness of the ozone layer, and have been calculated for various atmospheric conditions [12].

The photon flux calculated by Shettle and Green is presented in Table IV. The dramatic drop in background radiation levels at around 280 nm is evident. The signal that would be transmitted through a narrow band (10 nm) multilayer dielectric filter at 300 nm would include up to 10^{13} photons/cm² as background noise photons, whereas at

wavelengths below 280 nm this background radiation level may be considered to be quite small.

TABLE IV

Photon Flux Due to Direct and Diffuse Transmittance through the Earth's Atmosphere [12]

A solar angle of ninety degrees is assumed, along with a 0.32 cm ozone thickness.

λ (nm)	Flux (watts/m ² nm)	Flux (photons/cm ² nm sec)
300	1.07×10^{-2}	1.6×10^{12}
295	5.15×10^{-4}	7.8×10^{10}
290	2.14×10^{-6}	3.2×10^8
285	9.50×10^{-11}	1.4×10^4
280	9.09×10^{-19}	1.4×10^{-4}

D. DETECTOR CHARACTERISTICS

The detector characteristics which relate to a given S/N expression include filter characteristics, quantum efficiency, detector area, and field of view. Using a combination of multilayer dielectric filters and absorption filters, it is possible to construct a device having composite characteristics which will pass ten percent of the incident flux at 265 nm and reject the ambient solar flux in the visible to a degree sufficient to reduce the overall background count level to approximately ten counts per

second [29]. The transmission characteristics of this filter in the 200 to 400 nm region are indicated in Figure 15. It is thus expected that somewhat greater than one percent but less than ten percent of the photons in the 250 to 280 nm region will pass through the filter. Once the photons reach the photocathode of a typical photomultiplier, the conversion efficiency is usually greater than ten percent but less than 25 percent. Thus, for purposes of estimating S/N, the combined effects of filter transmission characteristics plus quantum efficiency of the photocathode may be accounted for by choosing a value of η to be greater than 10^{-3} but less than 10^{-2} . With unforeseen developments it is possible to expect a combination having a composite value of 10^{-1} , however such a device is not presently available.

The area of the detector used in the simulation was chosen to be nominally one square inch, typical of currently available photomultiplier tubes.

E. STATISTICAL CONSIDERATIONS

The number of photons converted into an electrical signal follows Poisson statistics:

$$P(r) = e^{-n} n^r / r! \quad (11)$$

where $P(r)$ is the probability that r photons are observed in a sample pulse which has an average number of n photons per pulse.

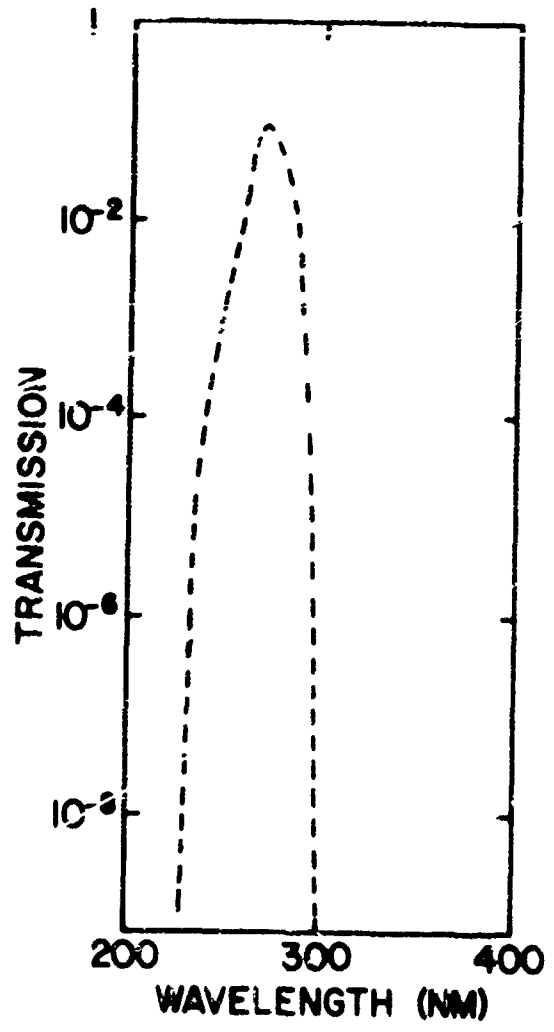


FIGURE 15. Transmission Characteristics for a Typical Composite Filter

The probability of observing an event with a number of photons above the threshold value r_{th} is

$$P(r > r_{th}) = \sum_{r=r_{th}}^{\infty} e^{-n} n^r / r! \quad (12)$$

Graphs of this function are readily available [30]. Given an average number, n , equal to ten and a threshold level of two (to distinguish from the random single photon events which occur at the detector with a frequency of occurrence equal to ten or twenty photons per second), a probability of detection of such pulses is .9995. If the average number n is five with the threshold number equal to two, the probability of detection is 0.96. Thus an average value of ten photons per pulse in the absence of background radiation is chosen as a desired level to avoid excessive error. This means that a desirable value of S/N is ten.

F. SUMMARY OF SIGNAL-TO-NOISE CONSIDERATIONS

For the case of minimal background radiation, Eq. (13) gives the relationship for the number of signal photons required.

$$\frac{P_s}{h\nu} = \frac{1}{n} \left(\frac{S}{N} \right) \quad (13)$$

If background radiation dominates the power incident on the detector (as would be the case at wavelengths longer than 300 nm), then the number of signal photons required is given by Eq. (14).

$$\frac{P_S \tau}{h\nu} = \left[\frac{1}{\eta} \left(\frac{S}{N} \right) \left(\frac{P_B \tau}{h\nu} \right) \right]^{1/2} \quad (14)$$

Table V gives a summary of the necessary photon flux external to the detector in order to obtain a S/N equal to ten. These flux levels may be used in conjunction with the figures of Section V to generate the geometric patterns over which signal transmission may be expected.

TABLE V

Photon Flux Required in order to Give
a S/N Equal to Ten

Assumed parameters:

Filter characteristics for Figure 15

Quantum efficiency of ten percent

$\tau = 10^{-6}$ seconds (significant pulse spreading)

Area of detector is one square inch

Note: Filter characteristics at 300 nm have been assumed for a narrow band (ten nm) multilayer dielectric filter.

λ (nm)	η	$\frac{P_B}{h\nu}$ (photons/sec)	$\frac{P_S \tau}{h\nu}$ (photons)	Required flux (photons/cm ²)
250	10^{-3}	---	10^4	1.6×10^3
265	10^{-2}	---	10^3	1.6×10^2
280	10^{-3}	---	10^4	1.6×10^3
300	10^{-2}	10^{13}	10^5	1.6×10^4

VII. DISCUSSION

Although not currently available, three millijoule laser sources of different wavelengths (250, 280, and 300 nanometers) capable of being pulsed at an appropriate rate (200 pulses per second for 2400 bit per second data rate using 12 bits per pulse [4]) were assumed. (The navy has used vocoders with 2400 bits per second capability since the 1940's). Table V lists the assumptions leading to the required photon flux in order to achieve a S/N equal to ten. By utilizing the contours of equal photon flux in Figures 8, 9, and 10, the ranges for which pulse position modulation communication is possible were predicted. Table VI lists the results of these calculations.

Predicted performance for lasers operating at 250 and 280 nm are comparable for sixty degree or greater off axis detection. For detection angles less than sixty degrees the 280 nm laser is superior. The performance of the 300 nm laser does not appear to be degraded by the background radiation as much as might be expected. The performance for this laser from zero to twenty degrees off from the axis of propagation is similar to the 280 nm laser. Beyond thirty degrees the ranges decrease markedly, indicating very little backscattering. It cannot be overstressed that the results above are for a simulation of assumed laser sources with assumed atmospheric propagation

TABLE VI

Predicted Ranges or Range Bands for Communication in the Middle UV for Pulsed Millijoule Lasers

(θ is the angular location of the receiver with respect to the axis of propagation.)

$\lambda = 250\text{nm}$ ($1.6 \times 10^3 \frac{\text{Photons}}{\text{cm}^2} \text{ req'd}$) $\lambda = 280\text{nm}$ ($1.6 \times 10^3 \frac{\text{Photons}}{\text{cm}^2} \text{ req'd}$) $\lambda = 300\text{nm}$ ($1.6 \times 10^4 \frac{\text{Photons}}{\text{cm}^2} \text{ req'd}$)

$5000 \frac{\text{Photons}}{\text{cm}^2}$		$500 \frac{\text{Photons}}{\text{cm}^2}$		$1526 \frac{\text{Photons}}{\text{cm}^2}$		$7875 \frac{\text{Photons}}{\text{cm}^2}$	
θ (Degrees)	Range (km)	Range (km)	Range (km)	θ (Degrees)	Range (km)	θ (Degrees)	Range (km)
0	2.4	3.4	5.5	0	5.2	0	5.2
30	1.1	2.1	2.9	30	2.9	10	3.6
60	.52	1.7	1.6	60	1.6	20	2.2
90	.34	1.2	1.0	90	1.0	30	.93
120	.30	1.0	.92	120	.92	40	.24
150	.33	1.1	.94	150	.94	90	.10
180	.49	1.2	1.2	180	1.2	180	.10

(Ranges for $\lambda = 250$ nm should be approximately half-way between the ranges listed.)

(Ranges for $\lambda = 280$ nm should be on the order of the range listed.)

(Ranges for $\lambda = 300$ nm should be somewhat less than the range listed.)

characteristics and assumed detector characteristics.
Clearly, in order to make accurate predictions for real systems it is necessary to obtain accurate atmospheric characteristics as well as other system parameters.

VIII. CONCLUSION

Lasers operating in the middle uv do not appear to be suitable for long range communications; however, they present definite possibilities for short range (several km) applications. Since radiation in this region is absorbed exponentially, rather than as the inverse of distance squared, the potential for covertness is highly accentuated. Current lasers, however, having a power output on the order of 0.1 joules or greater with low pulse rates (15 to 20 pulses per second), are not suitable for voice communication due to the low repetition rates. The pulsed mode of operation appears to hold definite advantages over amplitude modulation of a continuous wave laser from simple signal-to-noise considerations. Good possibilities for successful communication are offered by pulse position modulation. Millijoule laser sources operating with 200 or more pulses per second are desirable but not currently available.

The contours of equal photon flux presented in this paper are useful for determining the communication patterns of possible laser sources. The pulse spreading and field of view figures are likewise useful for predicting the characteristics of proposed receivers. A multiple scattering model is definitely required for proper prediction of photon flux over expected distances of communication.

APPENDIX A

MONTE CARLO SIMULATION OF THE
MULTIPLE SCATTERING PROBLEM

A. FUNDAMENTAL RELATIONSHIPS

1. Weighting Factors for Monte Carlo Calculations

The following calculations served as a model for the derivation of the various weighting factors:

PROBLEM: Given a random number generator that provides numbers within a specified interval along the x-axis (with equal probability for each interval dx) obtain random numbers with a probability $p(y)$. I.e., Find $y(x)$ such that $p(y)dy = dx$.

SOLUTION: Let Random Variable Y be distributed in $Y_0 \leq Y \leq Y_2$ and its density function be given by

$$p(y) = \begin{cases} p(y) & Y_0 \leq Y \leq Y_2 \\ 0 & \text{otherwise} \end{cases}$$

The distribution function, $P(y)$, is given by

$$P(y) = P(Y \leq y) = \int_{-\infty}^y p(y) dy$$

Therefore, $P(y) = \int_{Y_0}^y p(y) dy$, since $p(y) = 0$ for $y < Y_0$.

Now,

$$p(y) dy = dx$$

Integrating,

$$y(x) = y_0 + P^{-1}(\Delta x)$$

where

$$y_0 = y(x_0)$$

and $\Delta x = x - x_0$

This concept applied to specific cases yields the following fundamental relationships for weighting factors:

a. Exponential

$$p(y) = \frac{1}{\tau} e^{-y/\tau} \quad (0 \leq y \leq \infty)$$

$$y(x) = -\tau \ln(1 - \Delta x)$$

b. Henyey-Greenstein

$$p(\theta) = \frac{(1-g^2)}{2(1+g^2-2g \cos \theta)^{3/2}} \quad (0 \leq \theta \leq \pi)$$

where

$$g = \langle \cos \theta \rangle$$

$$\theta(x) = \cos^{-1} \left\{ \frac{1+g^2}{2g} - \frac{1}{2g} \left[\frac{1-g^2}{2g \left(\frac{1+g}{2g} - \Delta x \right)} \right]^2 \right\}$$

c. Modified Henyey-Greenstein [Zachor 1977]

$$p(\theta) = \frac{1-g^2}{2} \left[\frac{1}{(1+g^2-2g \cos \theta)^{3/2}} + \frac{f}{2} \frac{(3 \cos^2 \theta - 1)}{(1+g^2)^{3/2}} \right]$$

$$0 \leq \theta \leq \pi$$

where

$g = \langle \cos \theta \rangle$ and f is a weighting factor.

$$\theta(x) = \cos^{-1} \left\{ \frac{1+g^2}{2g} - \left[\frac{(g^2-1)^2}{8g^3} \right] \frac{1}{[\Delta x - F(\theta) - \frac{1+g}{2g}]^2} \right\}$$

where

$$F(\theta) = \left[\frac{f}{4} \frac{(1-g^2)}{(1+g^2)^{3/2}} \right] (\cos \theta - \cos^3 \theta)$$

d. Uniform

$$p(\phi) = \frac{1}{2\pi} \quad 0 \leq \phi \leq 2\pi$$

$$\phi(x) = 2\pi \Delta x$$

e. Rayleigh

$$p(\theta) = \frac{3}{8}(1 + \cos^2 \theta) \quad 0 \leq \theta \leq \pi$$

$$\theta(x) = \cos^{-1}(A + B)$$

where

$$A = \sqrt[3]{-\frac{b}{2} + \sqrt{\frac{b^2}{4} + 1}}$$

$$B = \sqrt[3]{-\frac{b}{2} - \sqrt{\frac{b^2}{4} + 1}}$$

and

$$b = 8 \Delta x - 4$$

2. Position and Coordinates in Photon-Fixed Coordinate System

a. Axis Rotation

Axis rotation is accomplished by the following transformation:

$$\begin{bmatrix} x' \\ y' \\ z' \end{bmatrix} = \begin{bmatrix} \cos \Delta\theta \cos \Delta\phi & -\cos \Delta\theta \sin \Delta\phi & -\sin \Delta\theta \\ \sin \Delta\phi & \cos \Delta\phi & 0 \\ \sin \Delta\theta \cos \Delta\phi & -\sin \Delta\theta \sin \Delta\phi & \cos \Delta\theta \end{bmatrix} \begin{bmatrix} x \\ y \\ z \end{bmatrix}$$

b. Axis Translation

Axis translation is accomplished by the following transformation:

$$\begin{bmatrix} x'' \\ y'' \\ z'' \end{bmatrix} = \begin{bmatrix} x' \\ y' \\ z' \end{bmatrix} + \Delta r \begin{bmatrix} 0 \\ 0 \\ 1 \end{bmatrix}$$

3. Angles ($\theta, \phi, \theta', \phi'$) for a Photon Passing Through a Shell¹

A laser is located at the origin of the $\hat{i}_0, \hat{j}_0, \hat{k}_0$ coordinate system. The initial direction of propagation of the collimated beam is along the $-\hat{k}_0$ axis. θ is the angle between the position vector \bar{R} (pointing from the location where the photon penetrates a shell toward the laser source) and the vector $-\hat{k}_0$. ϕ is the angle between the projection of $-\bar{R}$ onto the (\hat{i}_0, \hat{j}_0) plane (denoted by $-\bar{R}_p$) and the vector \hat{i}_0 .

A photon is located at the origin of the $\hat{V}_x, \hat{V}_y, \hat{V}_z$ and the $\hat{U}_x, \hat{U}_y, \hat{U}_z$ coordinate systems. As the photon passes through the shell, θ' specifies the angular direction of photon travel (along \hat{U}_z) relative to \bar{R} (the line-of-sight position vector). ϕ' is the angle between the projection of \bar{U}_z (denoted by the vector \bar{W}) onto the (\hat{V}_x, \hat{V}_y) plane and \hat{V}_x .

The vectors $\bar{R}_i, \bar{R}_j,$ and \bar{R}_k are position vectors in the $\hat{U}_x, \hat{U}_y, \hat{U}_z$ coordinate system denoting the location of the points $(1,0,0), (0,1,0),$ and $(0,0,1)$ in the $\hat{i}_0, \hat{j}_0,$

¹See Figure 16.

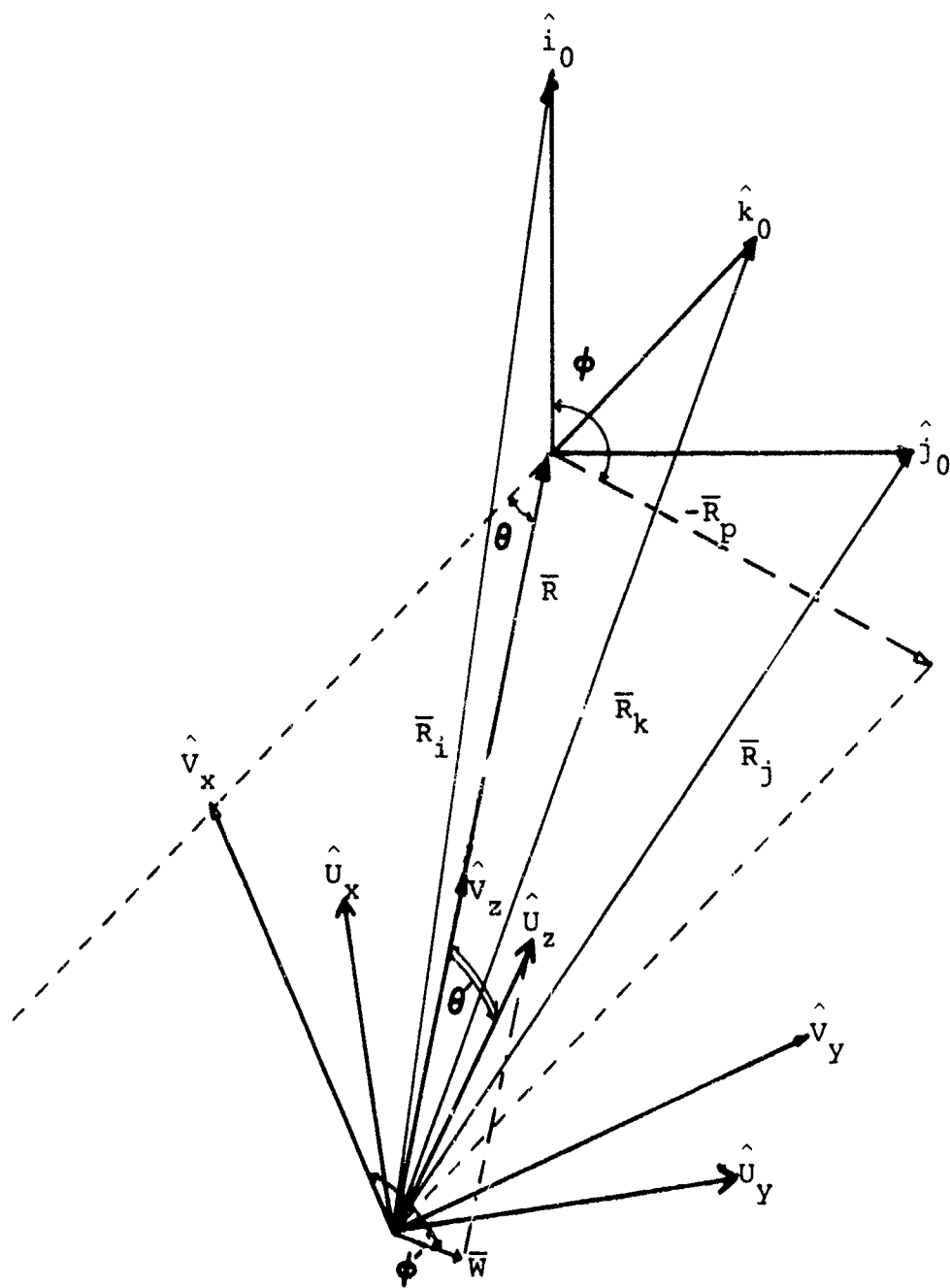


FIGURE 16. Diagram of the Photon Fixed Coordinate System

\hat{k}_o coordinate system. (These points are used for orientation purposes.)

$$\text{a. } \theta = \cos^{-1} \left(\frac{\bar{R} \cdot \hat{k}_o}{|\bar{R}| |\hat{k}_o|} \right)$$

$$\theta = \cos^{-1} \left[\frac{\bar{R} \cdot (\bar{R}_k - \bar{R})}{r} \right] \quad (0 \leq \theta \leq \pi)$$

$$\text{b. } \phi = \cos^{-1} \left(\frac{\bar{R} \cdot \hat{i}_o}{|\bar{R}_p|} \right)$$

$$\phi = \cos^{-1} \left[\frac{\bar{R} \cdot (\bar{R}_i - \bar{R})}{r_p} \right]$$

where

$$r_p = \sqrt{r^2 - [(\bar{R}_k - \bar{R}) \cdot \bar{R}]^2} \quad (0 \leq \phi \leq 2\pi)$$

$$\text{c. } \theta' = \cos^{-1} \left(\frac{\hat{U}_z \cdot \bar{R}}{|\bar{R}|} \right)$$

$$\theta' = \cos^{-1} \left(\frac{\hat{U}_z \cdot \bar{R}}{r} \right) \quad (0 \leq \theta' \leq \pi)$$

$$\text{d. } \phi' = \cos^{-1} \left(\frac{\hat{V}_x \cdot \bar{W}}{w} \right) \quad (0 \leq \phi' \leq 2\pi)$$

where

$$w = 1 - (\hat{V}_z \cdot \hat{U}_z)^2$$

4. Mapping Spherical Coordinates onto Polar Coordinates and Coordinate Transformation

In order to map a point on a sphere onto a circle(s) such that there is a one-to-one mapping the following transformations were utilized:

Case I. $0 \leq \theta \leq \pi/2$

$$r = R \sqrt{1 - \cos \theta}$$

$$\theta = \cos^{-1} \left[1 - \left(\frac{r}{R}\right)^2 \right]$$

Case II. $\pi/2 \leq \theta \leq \pi$

$$r = R \sqrt{1 + \cos \theta}$$

$$\theta = \cos^{-1} \left[\left(\frac{r}{R}\right)^2 - 1 \right]$$

In order to plot (θ, ϕ) the following coordinate transformation was used:

I.e. - Given (θ, ϕ) , find (x, y) .

$$r = \begin{cases} R \sqrt{1 - \cos \theta} & 0 \leq \theta \leq \pi/2 \\ R \sqrt{1 + \cos \theta} & \pi/2 \leq \theta \leq \pi \end{cases}$$

$$x = r \cos \phi$$

$$y = r \sin \phi$$

5. Phase Functions

A factor of $(\frac{1}{2\pi})$ arises from the normalization process for the phase function.

$$\text{(i.e. } \int_0^{2\pi} \int_0^{\pi} p(\theta) \sin\theta d\theta d\phi = 1)$$

a. Particulate

$$P(\theta) = \frac{1-g^2}{4\pi} \left[\frac{1}{(1+g^2-2g \cos \theta)^{3/2}} + \frac{g}{2} \frac{3 \cos^2 \theta - 1}{(1+g^2)^{3/2}} \right]$$

b. Rayleigh

$$P(\theta) = \frac{3}{16\pi} (1 + \cos^2 \theta)$$

APPENDIX B

DEVELOPMENT OF THE FUNDAMENTAL RELATIONSHIP
FOR RAYLEIGH SCATTERING

$$p(\theta) = \frac{3}{8} (1 + \cos^2 \theta) \quad 0 \leq \theta \leq \pi$$

$$\begin{aligned} x &= \int_0^\theta p(\theta) d \cos \theta \\ &= \int_0^\theta \frac{3}{8} (1 + \cos^2 \theta) d \cos \theta \\ &= -\frac{3}{8} \left(\cos \theta + \frac{\cos^3 \theta}{3} \right) \Big|_0^\theta \end{aligned}$$

$$x = -\frac{3}{8} \left(\cos \theta + \frac{\cos^3 \theta}{3} \right) + \frac{1}{2}$$

Now solve for $\cos \theta$.

$$\cos^3 \theta + 3 \cos \theta + (8x - 4) = 0$$

Let

$$y = \cos \theta$$

$$b = 8x - 4$$

$$a = 3$$

$$y^3 + ay + 6 = 0$$

(See Reference 31 for the solution to a cubic equation.)

$$y = A + B$$

or

$$y = -\frac{A+B}{2} + \frac{A-B}{2}\sqrt{-3}$$

or

$$y = -\frac{A+B}{2} - \frac{A-B}{2}\sqrt{-3}$$

where

$$A = \sqrt[3]{-\frac{b}{2} + \sqrt{\frac{b^2}{4} + \frac{a^3}{27}}}$$

and

$$B = \sqrt[3]{-\frac{b}{2} - \sqrt{\frac{b^2}{4} + \frac{a^3}{27}}}$$

Now

$$\frac{b^2}{4} + \frac{a^3}{27} = \frac{b^2}{4} + \frac{3^3}{27} = \frac{b^2}{4} + 1$$

$$\frac{b^2}{4} \geq 0; \quad \frac{b^2}{4} + 1 > 0$$

Therefore, only one real root and two conjugate imaginary roots exist.

Since $y = \cos \theta$, only one real root is considered.

$$\theta = \cos^{-1}(A + B)$$

where

$$A = \sqrt[3]{-\frac{b}{2} + \sqrt{\frac{b^2}{4} + 1}}$$

$$B = \sqrt[3]{-\frac{b}{2} - \sqrt{\frac{b^2}{4} + 1}}$$

and

$$b = 8x - 4$$

APPENDIX C

SAMPLE CALCULATION FOR RANGE PREDICTION

PROBLEM: Given a single channel 280 nm laser utilizing pulse position with power output per pulse equal to one millijoule, determine the communication pattern for a S/N equal to ten. Assume the detector characteristics presented in Section VI.

SOLUTION: From Table V, the minimum photon flux for a S/N of ten is 1.6×10^3 photons per cm^2 .

Now,

$$1 \text{ watt} = 5.0345 \times 10^{18} \lambda \frac{\text{photons}}{\text{sec}}$$

where

$$\lambda = .280 \quad (\lambda \text{ is measured in } \mu)$$

$$1 \text{ joule} = 1 \text{ watt sec}$$

$$= 1.40966 \times 10^{18} \text{ photons}$$

$$1 \text{ millijoule} = 1.40966 \times 10^{15} \text{ photons}$$

From Figure 9, at contour 2 the relative flux is 10^{-2} of the initial photons per unit area where the unit area is one extinction length squared. From Table III one extinction length is

(1.0405 km^{-1})⁻¹ or .9611 kilometers. The relative flux is $1.0826 \times 10^{-12} \text{ cm}^{-2}$. The irradiance is given by the product of 1.40966×10^{15} and 1.0826×10^{-12} or 1526 photons per square cm. By measuring the distance from the source to the detector located on contour 2 (Figure 9) and recalling that one extinction length for this case is .9611 km, the ranges for an irradiance of 1526 photons/cm² may be determined. Table VI lists the results of this calculation.

APPENDIX D

CHECKS ON POSSIBLE ERRORS

Each computational procedure involved in writing this program was verified and an effort was made to ensure the entire program functioned properly. The procedures utilized to document the correct behavior of this routine are described in this appendix.

The various weighting functions in the program were verified by comparing the actual distribution of photons generated by the computer to the analytical solution for the distribution of random numbers obtained using a programmable calculator. (The statements required for this generation remain in the program, but the output of the results is suppressed.)

Verification of axis transformation computations was simple and straight-forward. The axes were rotated about the Z axis, the Y axis, and finally about both axes to ensure proper behavior. (No documentation steps of this nature have been left in the program.) The output of θ , ξ , η , and ϕ for each photon at each shell was ordered by a computer sort routine in order to facilitate the preparation of a scatter diagram indicating the pattern formed by the simulated photons. Inspection of such a pattern did in fact reveal the presence of a fault which was corrected.

The results of Duntley [32] in describing multiply scattered radiation in the propagation of laser light under water are most useful. Flux as a function of cone angle is presented for distances of up to 19 attenuation lengths. The scattering phase function for light underwater is a sharply peaked function which may be approximated with a Henyey-Greenstein function with a g value equal to 0.96 [33]. Calculations of photon flux as a function of cone angle were carried out with the computer program developed. Total attenuation of the beam down to a level of 10^{-3} could be calculated with some measure of accuracy (only 10,000 simulated photons were utilized for these calculations.) The results of these calculations agreed with the behavior observed in these underwater scattering measurements, simulating correctly the flux levels out to 16 attenuation lengths (the limit calculated).

Further verification of the accuracy of the program was obtained by comparison with calculations by Zachor and Green [24]. In this article, photon flux as a function of viewing angle was calculated for several distances from the source. The same conditions were assumed with the model used here, resulting in satisfactory agreement with the information published by Zachor for distances of 1.43, 2.73, and 4.95 extinction lengths for 300 nm radiation.

APPENDIX E

PROGRAM DESCRIPTION AND DOCUMENTATION

A. COMPONENTS OF THE PROGRAM

1. Weighting Function Subprograms

RANEXP is a function subprogram that generates random numbers weighted exponentially. It is used for distance calculations.

Function subprogram RANTH generates random values for theta and theta prime. Since the interaction may be either Rayleigh scattering or particulate scattering, either calculation may be performed. A uniform random number (generated by RANDU) within the interval [0,1] is obtained and compared to R_p (the ratio of particulate to total scattering). If the random number is less than R_p the particulate scattering calculation is made. (Otherwise the Rayleigh calculation is performed.) Due to the complexity of the particulate phase function it is difficult to obtain an exact solution; therefore an iterative method is employed. An exact solution is available when f is set to zero and a more efficient calculation is utilized.

RANPH generates a random value of phi or phi prime uniformly weighted on the interval $[0, 2\pi]$. The steps in this function subprogram are trivial.

2. LITE Subroutine

The main subroutine of the Monte Carlo simulation, called LITE, simulates a photon which randomly interacts with atmospheric constituents. (In order to make the most efficient use of computer time, non-interaction was not considered.) Initially the photon travels along the $-K_0$ axis (see Figure 16, Appendix A), a distance ΔR (determined by function subprogram RANEXP). A uniform random variable in the interval $[0,1]$ is compared to R_S (the ratio of the total scattering coefficient, K_S , to the total extinction coefficient, K). If the random number is smaller than R_S , the photon is scattered. (Otherwise it is absorbed and the photon is lost.) If it is scattered, the distance of the photon from the laser is updated and a new value of R is calculated. Since the photon has been scattered, new angles and distances must be computed. This is accomplished by generating values for $\Delta\theta$, $\Delta\phi$, and ΔR (using RANTH, RANPH, and RANEXP, respectively). The photon coordinate system is transformed (translated and rotated) to a new coordinate system. The distance from the source is calculated and compared with the radius of a shell. (A series of concentric shells with radii measured in extinction lengths, may be formed in order to determine the photon flux or angular distribution of photons as a function of distance from the source.) Various calculations are then made to determine whether a photon has penetrated through a shell, passed in and out of a shell, or penetrated an outer shell. These calculations are necessary to ensure proper accounting of

the photon flux. When a photon passes through a shell, the position of the source with respect to the penetration point is obtained. Theta, phi, and the radius of the shell (measured in extinction lengths) are stored in a three dimensional array for future use. Theta prime and phi prime are also determined as a function of distance (using RANTH and RANPH). These too, are stored in a three dimensional array and specify the direction of incident photon flux as observed by a receiver located a given distance from the source at a given angle off from the axis of propagation. This process is repeated until all of the photons have been used to generate information. (It should be noted that many extra steps incorporated to debug the program, remain in to facilitate future implementation by another user.)

3. DRLITE Routine

The routine DRLITE is used to drive the subroutine LITE. Information is read into the computer and the results are written out using this routine. The spatial distribution of photons as a function of position and detector field of view is calculated as well as the total number of photons in each shell. The output of other available information is optional and is controlled by IPRT and METHOD statements. This information includes pulse spreading (or photon time of arrival) as a function of position and field of view, the relative photon flux at each annular ring in a shell,

and a least square curve fitting of a modified Henyey-Greenstein function to the phase function information generated by the computer.

4. Miscellaneous Subroutines and Function Subprograms

LSTHG, LEAST, GAUSS3, and RANDU are miscellaneous subroutines used in the program. LSTHG is used to least squares fit a modified Henyey-Greenstein function to the information generated. LEAST and GAUSS3 are used in conjunction with LSTHG. EQN is a function subprogram supporting LSTHG. RANDU is a uniform random number generator that provides numbers in the interval [0,1]. It is located in the computer library. The variable IX is the seed and may be any odd integer with nine digits or less. It may not be zero. In order to use RANDU the following FORTRAN statements are used:

```
IX = 948752759
CALL RANDU (IX,IY,Y)
IX = IY
```

The seed IX is used in the calculation and a new seed IY is generated for future use. A uniform random number, Y, is in the interval [0,1] and is also available for future calculations. The last statement (IX = IY) resets the seed IX to a new value.

DR1000010
DR1000020
DR1000030
DR1000040
DR1000050
DR1000060
DR1000070
DR1000080
DR1000090
DR1000100
DR1000110
DR1000120
DR1000130
DR1000140
DR1000150
DR1000160
DR1000170
DR1000180
DR1000190
DR1000200
DR1000210
DR1000220
DR1000230
DR1000240
DR1000250
DR1000260
DR1000270
DR1000280
DR1000290
DR1000300
DR1000310
DR1000320
DR1000330
DR1000340
DR1000350
DR1000360
DR1000370
DR1000380
DR1000390
DR1000400
DR1000410
DR1000420
DR1000430
DR1000440
DR1000450
DR1000460
DR1000470
DR1000480

THIS ROUTINE IS INTENDED TO DRIVE THE MONTE CARLO ROUTINE
CALLED LITE, WHICH CALCULATES THE DISTRIBUTION OF PHOTONS
FROM A UNIFORM LIGHT SOURCE. IT IS USED TO READ
INFORMATION INTO THE PROGRAM AND TO CONTROL THE OUTPUT.
THE DISTRIBUTION OF PHOTONS AND THE TOTAL NUMBER OF PHO-
TONS IN EACH SHELL ARE STANDARD BY METHOD AND STATE-
MENTS. LITE IS CONTROLLED BY METHOD AND IPRMRT STATE-
MENTS. IPRMRT CONTROLS THE SHAPE OF THE THETA BINS,
WHILE IPRMRT CONTROLS THE ACTUAL OUTPUT.

IPRT = 0,1,2,3,4,5,6,7,8, CR 5 YIELDS THE STANDARD
OUTPUT.
IPRT = 1,2,3,4, CR 5 YIELDS THE NEGATIVE LOG CF
RELATIVE FLUX AT EACH ANNUAL RING.
IPRT = 3,4,5,6,7,8, OR 9 YIELDS THE TIME OF ARRIVAL
OR PULSE SPREADING INFORMATION.
IPRT = 6,7,8, OR 9 YIELDS A LEAST SQUARE FIT TO A
MODIFIED HENY-GREENSTEIN FUNCTION TO THE
PHASE FUNCTION INFORMATION.

```

REAL*8 GIN BINS(20,50,1), BINDST(20,50,20)
INTEGER*4 RFLUX(20,50,1)
EQUIVALENCE (BINS,RFLUX)
DATA PI/3.1415926536/
1  WCRMAT(1,500)
* IPRMRT(1,NPHOT,NTHETA,NFLDVM,NSHLS,METHOD,IX,CISTSH,RATIO,
500  G,RPT,RBACK,GIN,/)
* IPRMRT(5,505,NPHOT,NTHETA,NFLDVM,NSHLS,IFRT,METHOD,IX,
505  CISTSH,RATIO,G,RPT,RBACK,GIN)
IF(METHOD.EQ.0) METHOD = 1
IF(NPHOT.EQ.0) STOP
WRITE(6,110)
FCRMAT(1,110)
CALL LITE(NPHOT,NTHETA,NFLDVM,NSHLS,DISTSH,RATIO,G,RPT,RBACK,
* IX,BINS,BIN)
FCRMAT(1,515)
DCR50 I = 1,NSHLS
ISUM = 0
DO 44 J = 1,NTHETA
DO 44 K = 1,NFLDVM
ISUM = ISUM + BINS(I,J,K)
ICNTINUE = 520)
WRITE(6,IX)
520  WCRMAT(6,440) I,ISUM

```

CCCCCCCCCCCCCCCCCCCC

```

44C FCRMAT(IX,'TOTAL NUMBER IN SHELL ',I2,' IS ',I6)
   IF(NFLDVM.EC.1) GC TC 47
   DC 46 J=1,NTHETA
   ISUM = 0
   DC 45 K=1,NFLDVM
   ISUM = ISUM + BINS(I,J,K)
44I WRITE(6,441) J,ISUM
   FCRMAT(,' NO. IN BIN ',I2,' IS',I6)
4C  WRITE(6,521)(BINS(I,J,K),K=1,NFLDVM)
   CONTINUE
47  WRITE(6,521) ((BINS(I,J,K), K = 1,NFLDVM), J = 1,NTHETA)
4E  CONTINUE.LE.2) GO TO 5C
   IF(IPRT.LE.442)
442  FCRMAT(,' TIME OF ARRIVAL BINS GIVEN BY',/)
   DC 45 J = 1,NTHETA
45  WRITE(6,522) (BINDST(I,J,K), K = 1,20)
522  FCRMAT(IX,2CI6)
5C  CONTINUE
   GE.6) GO TC 399
   IF(IPRT.LE.1) GO TO 1
   IF(IPRT.LE.450)
45C  FCRMAT(,' RING IS',)
   DC 60 I = 1,NSHLS
   R = DISTSH*I
   DC 55 J = 1,NTHETA
   TF1 = (PI*(J-1))/NTHETA
   IF(METHOD.EC.3) TH1 = (TH1*(J-1))/NTHETA
   TF2 = (PI*J)/NTHETA
   IF(METHOD.EC.3) TH2 = (TH2*J)/NTHETA
   AREA = 2.0*PI*R**2*(COS(TH1)-COS(TH2))
   FCRMAT(,' SHELL ',I2,' THE AREA IS',F10.6)
   DC 55 K = 1,NFLDVM
   IF(BINS(I,J,K).EQ.0) RFLUX(I,J,K) = 0.0
   IF(BINS(I,J,K).EQ.0) GO TO 55
   RFLUX(I,J,K) = -ALCG10(BINS(I,J,K)/(AREA*NPCT))
   CONTINUE
55  WRITE(6,452) ((RFLUX(I,J,K), K = 1,NFLDVM),J = 1,NTHETA)
452  FCRMAT(IX,2CF6.2)
5C  CONTINUE
521  FCRMAT(IX,2CI6) GO TC 1
355  IF(IPRT.LE.5) GO TC 1
400  CALL LSTHG(NTHETA,NN,BINS,METHOD,GIN)
      GC TO 1

```

```

DR L00450
DR L00500
DR L00510
DR L00520
DR L00530
DR L00540
DR L00550
DR L00560
DR L00570
DR L00580
DR L00590
DR L00600
DR L00610
DR L00620
DR L00630
DR L00640
DR L00650
DR L00660
DR L00670
DR L00680
DR L00690
DR L00700
DR L00710
DR L00720
DR L00730
DR L00740
DR L00750
DR L00760
DR L00770
DR L00780
DR L00790
DR L00800
DR L00810
DR L00820
DR L00830
DR L00840
DR L00850
DR L00860
DR L00870
DR L00880
DR L00890
DR L00900
DR L00910
DR L00920
DR L00930
DR L00940
DR L00950
DR L00956

```

DR L0057C

ENC

```

C****
FUNCTION HANEXP(IX,IY,TAU)
THIS FUNCTION GENERATES A RANDOM NUMBER WEICHTED EXPONENTIALLY
CALL RANDU(IX,IY,RN)
IX = IY
RANEXP = -TAU*ALCG(1.0-RN)
RETURN
END

C
FUNCTION RANTH(IX,IY,HENA,HENB,HENC,HEND,RPT,FBACK)
THIS FUNCTION GENERATES A RANDOM VALUE OF THETA,
SUITABLY WEIGHTED
DATA PI2/1.5707963268/, PI/3.1415926536/
IX = IY
IF(RN.GT.RPT) GO TO 20
IF(FBACK.EQ.0.0) GO TO 10
CALL RANDU(IX,IY,RN)
IX = IY
CRANM1 = 0.0
CC 5
CRANTH = HENA-HENB/(RN-HENC-HEND*FBACK*CRANM1*(1.0-CRANM1)**2)**2
WRITE(6,999) I,CRANTH,RN
*CFRMT(IX,14,2F12.6)
IF(ABS(CRANTH-CRANM1).LT.0.001) GO TO 8
CRANM2 = CRANM1
CRANM1 = CRANTH
CCNTINUE
CRANTH = 0.25*(CRANM2+CRANTH)+0.01*CRANM1
WRITE(7,998) CRANTH,RN
*CFRMT(IX,2F10.6)
CCNTINUE
IF(ABS(CRANTH).GT.1.0) CRANTH = CRANTH/(ABS(CRANTH) + .00001)
RETURN
CALCULATE THETA USING FORWARD SCATTER FUNCTION HERE
CALL RANDU(IX,IY,RN)
IX = IY
WRITE(6,990) HENA,HENB,HENC,RN
*CFRMT(IX,4F12.6)
RANTH = ARCCS(HENA-HENB/(HENC-RN)**2)
RETURN
CALCULATE THETA ASSUMING RAYLEIGH SCATTERING HERE
CALL RANDU(IX,IY,RN)
IX = IY
RLB = 4.0*RN-2.0
RLBS = SQRT(RLB**2-1.0)
CAPA = (-RLB+RLBS)**(1./3.)
CAPB = -(RLB+RLBS)**(1./3.)

```

```

FUNCO 110
FUNCO 120
FUNCO 130
FUNCO 140
FUNCO 150
FUNCO 160
FUNCO 170
FUNCO 180
FUNCO 190
FUNCO 200
FUNCO 210
FUNCO 220
FUNCO 230
FUNCO 240
FUNCO 250
FUNCO 260
FUNCO 270
FUNCO 280
FUNCO 290
FUNCO 300
FUNCO 310
FUNCO 320
FUNCO 330
FUNCO 340
FUNCO 350
FUNCO 360
FUNCO 370
FUNCO 380
FUNCO 390
FUNCO 400
FUNCO 410
FUNCO 420
FUNCO 430
FUNCO 440
FUNCO 450
FUNCO 460
FUNCO 470
FUNCO 480

```

```
C
C***
RANTH = ARCCS(CAPA+CAPB)
RETURN
END
FUNCTION RANPH(IX,IY)
THIS FUNCTION GENERATES A RANDOM VALUE OF PHI
DATA TPI/6.283183072/
CALL RANDU(IX,IY,RN)
IX = IY
RANPH = TPI*RN
RETURN
END
```

```
FUNCC49C
FUN00500
FUN00510
FUN00520
FUN00530
FUN00540
FUN00550
FUN00560
FUN00570
FUN00580
FUNCC590
FUN00600
```

THIS SUBROUTINE SIMULATES A PHOTON WHICH PANGCMY COLLIDES WITH PARTICLES, SCATTERED AT ANGLES WEIGHTED BY VARIOUS FUNCTIONS, AND DETERMINES LOCATION OF INTERSECTION WITH VARIOUS SPHERES

INPUT PARAMETERS:

NPHOT = NUMBER OF PHOTONS TO TRACE THROUGH
 NTHETA = THE NUMBER OF THETA "BINS" TO KEEP TRACK OF
 NFLDVM = THE NUMBER OF "FIELD OF VIEW BINS" FOR EACH THETA BIN
 NSHLS = THE NUMBER OF SHELLS TO BE INTERSECTED BY EACH PHOTON
 DISTSH = THE DISTANCE BETWEEN EACH SHELL (AND FROM CRIGIN FOR FIRST)
 RATIC = RATIO OF SCATTERING CROSS SECTION TO TOTAL EXTINGUISH
 G = VALUE FOR HENY-GREENSTEIN FUNCTION
 FRPT = RATIO OF PARTICULATE TO TOTAL SCATTERING
 FRACK = RATIO OF BACKSCATTER TO TOTAL PARTICULATE SCATTERING
 IX IS A RANDOM NUMBER TO START THINGS

VARIABLES:
 X(I) = X COORDINATE; I=1 FOR ORIGIN, I=2 FOR X=1, I=3 FOR Z=1
 Y(I) = Y COORDINATE; (1,0,0) POINT FOR ORIGINAL COORD SYST, ETC.)
 Z(I) = Z COORDINATE; "DITTO"
 XT(I) = THE NEW COORDINATE AFTER ROTATION BY THETA, PHI, AND TRANSLATION BY DISTANCE DR

YT(I), AND ZT(I), LIKEWISE
 XS(I) IS A TEMPORARY COORDINATE POINT, AT THE INTERSECTION WITH THE SPHERE
 YS(I), ZS(I), LIKEWISE
 TP = AFTER SIMULATION WHICH COORDINATE SYSTEM IS ROTATED
 PH = VALUE OF THETA, PHI, LIKEWISE
 THP = VALUE OF THETA PRIME, THETA RELATIVE TO PHOTON-FIXED COORDINATE SYSTEM

PHR = VALUE OF THETA PRIME, IN PHOTON FIXED COORD SYST
 BINS(I, J, K) = NO OF OCCURRENCES AT THETA BIN J, THETA PRIME K, RSHL(I) = DISTANCE OF THETA BIN FROM ORIGIN
 LGTHA = NEW VALUE OF THETA RELATIVE TO OLD DIRECTION
 DPHI = NEW VALUE OF PHI RELATIVE TO OLD DIRECTION
 DR = DISTANCE OF PHOTON TRAVEL AFTER A COLLISION
 IXACT = FIXED POINT RANDOM NUMBERS
 DIST = TOTAL DISTANCE FROM ORIGIN OF PHOTON TRAVEL
 SCIST = DISTANCE FROM ORIGIN FOR PREVIOUS CALCULATION
 PCIST = DISTANCE ACTUALLY TRAVELED FROM ORIGIN TO SPELL
 ISAV = INTEGER CORRESPONDING TO NUMBER OF SHELL BEYOND WHICH THE PHOTON IS LOCATED
 XPCR = RATIO OF DISTANCE FROM POINT OF COLLISION TO A

DR100010
 DR100020
 DR100030
 DR100040
 DR100050
 DR100060
 DR100070
 DR100080
 DR100090
 DR100100
 DR100110
 DR100120
 DR100130
 DR100140
 DR100150
 DR100160
 DR100170
 DR100180
 DR100190
 DR100200
 DR100210
 DR100220
 DR100230
 DR100240
 DR100250
 DR100260
 DR100270
 DR100280
 DR100290
 DR100300
 DR100310
 DR100320
 DR100330
 DR100340
 DR100350
 DR100360
 DR100370
 DR100380
 DR100390
 DR100400
 DR100410
 DR100420
 DR100430
 DR100440
 DR100450
 DR100460
 DR100470
 DR100480

CC


```

C*** 25 IF PHOTON HAS PENETRATED CUTER SHELLS
C*** 26 IF (ISAV).GT.(NSHLS)) GO TO 100
C*** 27 IF (DIST.GT.RSHL(ISAV+1)) GO TO 5C
ISAV = ISAV-1
GO TO 37
C*** 40 UPDATE COORDINATES - GET READY FOR ANOTHER COLLISION
TIME TO RTCT+DR
SDIST = DIST+4
CX(I) = XT(I)
Y(I) = YT(I)
Z(I) = ZT(I)
CONTINUE
C*** 45 FOR ANOTHER COLLISION
GO TO 20
C*** 50 CALCULATE COORDINATES OF POINT AT WHICH PHOTON PENETRATES SHELL
ISAVE = ISAV+1 DR,ZT(I) **,.2F10.5)
WRITE(6,*) DR,ZT(I) **,.2F10.5)
CP 551 FCRMAT(6,*) SDIST,RSHL(ISAV) **,.2F10.5)
CP 552 FCRMAT(6,*) DIST,RTCT,ISAV **,.2F10.5,2X,I2)
CP 553 FCRMAT(6,*) DIST,RTCT,ISAV **,.2F10.5,2X,I2)
CP 554 FCRMAT(6,*) DR,ZT(I)-DR)**2+RSHL(ISAV)**2)/CR
WRITE(6,*) XPCR = ,F10.5)
FCRMAT(6,*) XPCR = ,F10.5)
CP 555 X(I) = XT(I)
Y(I) = YT(I)
Z(I) = ZT(I) - ((1.0-XPCR)*DK
CONTINUE
RTOT+XPDR*DR
CP 992 WRITE(6,992) (XS(I),YS(I),ZS(I), I = 1,4)
FCRMAT(6,*) COCRD. AT THETA
CALCULATE VALUE OF THETA
V + ZS(I)*((XS(I)-XS(3)) + YS(I)*((YS(1)-YS(3))
IF (ABS(VAL).GT.1.0) CALL PERR(I,IXS,VAL,XS,YS,ZS)
IF (ABS(VAL).GT.1.0) WRITE(6,200) VAL,NPH,IXS
FCRMAT(6,*) ARCOS GT. 1.0: VAL = ,F10.5, NPH, IXS = ,
* I10)
CP * IF (VAL.GT.1.0) VAL = 1.0
IF (VAL.LT.-1.0) VAL = -1.0
IF (TH.PI - ARCS(VAL)
IF (TH.LT.0.0) TH = 0.0
WRITE(6,995) RSHL(ISAV)
CP

```

```

LC1450
DRLO1460
DRLO1470
DRLO1480
DRLO1490
DRLO1500
DRLO1510
DRLO1520
DRLO1530
DRLO1540
DRLO1550
DRLO1560
DRLO1570
DRLO1580
DRLO1590
DRLO1600
DRLO1610
DRLO1620
DRLO1630
DRLO1640
DRLO1650
DRLO1660
DRLO1670
DRLO1680
DRLO1690
DRLO1700
DRLO1710
DRLO1720
DRLO1730
DRLO1740
DRLO1750
DRLO1760
DRLO1770
DRLO1780
DRLO1790
DRLO1800
DRLO1810
DRLO1820
DRLO1830
DRLO1840
DRLO1850
DRLO1860
DRLO1870
DRLO1880
DRLO1890
DRLO1900
DRLO1910
DRLO1920

```

DR L01923C
 DR L01940C
 DR L01950C
 DR L01960C
 DR L01970C
 DR L01980C
 DR L01990C
 DR L02000C
 DR L02010C
 DR L02020C
 DR L02030C
 DR L02040C
 DR L02050C
 DR L02060C
 DR L02070C
 DR L02080C
 DR L02090C
 DR L02100C
 DR L02110C
 DR L02120C
 DR L02130C
 DR L02140C
 DR L02150C
 DR L02160C
 DR L02170C
 DR L02180C
 DR L02190C
 DR L02200C
 DR L02210C
 DR L02220C
 DR L02230C
 DR L02240C
 DR L02250C
 DR L02260C
 DR L02270C
 DR L02280C
 DR L02290C
 DR L02300C
 DR L02310C
 DR L02320C
 DR L02330C
 DR L02340C
 DR L02350C
 DR L02360C
 DR L02370C
 DR L02380C
 DR L02390C
 DR L02400C

```

SSS FCRMAT(, AAA, FIC.5)
C*** CALCULATE VALUE OF PHI
      DENOMS = (RSHL(ISAV))*#2 - (XS(1)*(XS(3))-XS(1)) + YS(1)*
      * (YS(3))-YS(1))*ZS(1))*#2)
      IF (DENOMS.LT.EPSIL) CALL PERR(5,IXS,DENOMS,XS,YS,ZS)
      IF (DENOM.SQRT(DENOMS) IXS
      * WRITE(6,996) DENOM,PH = 0.0
      IF (DENOM.EQ.0.0) GO TO 158
      IF (DENOM.EQ.0.0) ,F10.6,I10)
      * FCRMAT(, DENOM: XS(1)-XS(2)) + YS(1)*(YS(1))-YS(2)) +
      * ZS(1)*(XS(1))-ZS(2))/DENOM)
      IF (ABS(VAL).GT.1.1) CALL PERR(2,IXS,VAL,XS,YS,ZS)
      IF (ABS(VAL).GT.1.1) WRITE(6,200) VAL, NPH, IXS
      IF (VAL.LT.-1.0) VAL = -1.0
      * PH = ARCCOS(VAL)
      * IF (LT.0.0) PH = TPI-PH
      * CNTINLE 998)
      * WRITE(6,998)
      * FCRMAT(, BBA',)
      * CALCULATE VALUE OF THETA PRIME (RECEIVER)
      * VAL = (ZS(1))/RSHL(ISAV))
      * IF (ABS(VAL).GT.1.1) CALL PERR(3,IXS,VAL,XS,YS,ZS)
      * IF (ABS(VAL).GT.1.1) WRITE(6,200) VAL, NPH, IXS
      * IF (VAL.GT.1.0) VAL = 1.0
      * IF (VAL.LT.-1.0) VAL = -1.0
      * THP = ARCCS(VAL)
      * WRITE(6,997)
      * FCRMAT(, CCC',)
      * CALCULATE VALUE OF PHI PRIME (RECEIVER)
      * PARAM = (XS(1)*XS(3) + YS(1)*YS(3) + ZS(1)*ZS(3))/
      * (RSHL(ISAV))*SQRT(XS(2)**2 + YS(2)**2 + ZS(2)**2))
      * WRITE(6,911) IXS, PARAM
      * FCRMAT(, M.LT.0.999) GO TO 159
      * VAL TO 585
      * FCRMAT(, DENOM: XS(1)-XS(1))
      * GC = -RSHL(ISAV)**2/(XS(3)*XS(1)+YS(3)*YS(1)+ZS(3)*ZS(1))
      * YX(1) = XS(3)
      * VY(1) = YS(3)
      * VZ(1) = ZS(3)
      * ANCRM = SQRT(VX(1)**2+VY(1)**2+VZ(1)**2)
      * VY(1) = VY(1)/ANCRM
      * VZ(1) = VZ(1)/ANCRM
  
```



```

CCCCCCCCCCCCCCCCCCCCCCCCCCCCCCCCCCCCCCCCCCCCCCCCCCCCCCCCCCCC
WRITE 1, DIMENSION SUBPROGRAM TO CALCULATE THE FUNCTION TO BE LEAST SQUARED
DIMENSIONED TO AND CONTAINS THE PARAMETERS TO BE VARIED SUCH AS
PARAMETERS TO USE ONLY X, XB, NOF IS THE FUNCTION NUMBER -
PARAMETER PARTS OF THE EQUATION MEANING--
ARE TO BE FIT (FOR SEVERAL JOBS TO BE DONE)
THE DIMENSIONED PARAMETERS CONTAIN THE INDEPENDENT PARAMETERS
X(200), XB(200), AND XC(200) CONTAIN THE INDEPENDENT PARAMETERS
PARAMETERS, THE OBSERVED VALUES OF THE FUNCTION (THE OBSERVED
PARAMETERS) CONTAINS THE MAGNITUDE OF THE INCREMENTS FOR THE PARAMETERS
FINCR(I) THE PROGRAM MAY TAKE NUMERICAL DERIVATIVES WITH REASONABLE
SCALE FACTOR CONTAINS THE DIFFERENCE BETWEEN OBSERVED THE PARAMETERS
ITERATION CONTAINS THE ESTIMATES OF THE ERRORS OF THE PARAMETERS A(I)
FIRST INPUT CARD - WILL BE REPRODUCED ON OUTPUT USED FOR LABELING.
SECOND CARD - FORMAT(I2,I3,I2,I3,E10.2)
IS= NUMBER OF POINTS
NOF= FUNCTION NUMBER (SEE ABOVE)
NINP= NUMBER OF INDEPENDENT PARAMETERS
EPS= IS USED AS A CRITERION FOR CONVERGENCE. IF THE RELATIVE VALUE
CONVERGENCE IS REACHED.
SUBROUTINE REAL(I, NN, IBIN, NOF, XPMIN)
IMPLICIT REAL*4 (A-H, C-Z)
DIMENSION A(10), X(200), XB(200), XC(200), Z(200), FINCR(I),
1 CALL ERASE(I, IS)
2 Z(I) = 0.0
5 SUM = 1.0
5 SUM = SUM + Z(I)
7 INP = 1
7 INP = 1
7 EPSIL = .0001
7 GCNTIN = 7.8E8, NOF
7 A(1) = SUM
7 A(2) = .90
7 A(10) = 180./IS
8 A(1) = .8

```

CC


```

C 950 CACHED LEAST.)
C 955 FCALL LEAST(IR,IS,A,X,XB,XC,Z,FINCF,EPSIL,NCITR,RRG,NGF,R,E)
C 1000 WRITTE(6,109)
C 1005 FCRRMAT(1,REACH)
C 1010 WRITTE(6,110)
C 1015 WRITTE(6,111)
C 1020 WRITTE(6,112)
C 1025 WRITTE(6,113)
C 1030 WRITTE(6,114)
C 1035 WRITTE(6,115)
C 1040 WRITTE(6,116)
C 1045 WRITTE(6,117)
C 1050 WRITTE(6,118)
C 1055 WRITTE(6,119)
C 1060 WRITTE(6,120)
C 1065 WRITTE(6,121)
C 1070 WRITTE(6,122)
C 1075 WRITTE(6,123)
C 1080 RETURN
C 1085 FCRRMAT(12,13,12,13,E10.2)
C 1090 FCRRMAT(16F5.0)
C 1095 FCRRMAT(16F5.0)
C 1100 FCRRMAT(16F5.0)
C 1105 FCRRMAT(16F5.0)
C 1110 FCRRMAT(180)
C 1115 FCRRMAT(19H)
C 1120 FCRRMAT(19H)
C 1125 FCRRMAT(19H)
C 1130 FCRRMAT(19H)
C 1135 FCRRMAT(19H)
C 1140 FCRRMAT(19H)
C 1145 FCRRMAT(19H)
C 1150 FCRRMAT(19H)
C 1155 FCRRMAT(19H)
C 1160 FCRRMAT(19H)
C 1165 FCRRMAT(19H)
C 1170 FCRRMAT(19H)
C 1175 FCRRMAT(19H)
C 1180 FCRRMAT(19H)
C 1185 FCRRMAT(19H)
C 1190 FCRRMAT(19H)
C 1195 FCRRMAT(19H)
C 1200 FCRRMAT(19H)
C 1205 FCRRMAT(19H)
C 1210 FCRRMAT(19H)
C 1215 FCRRMAT(19H)
C 1220 FCRRMAT(19H)
C 1225 FCRRMAT(19H)
C 1230 FCRRMAT(19H)
C 1235 FCRRMAT(19H)
C 1240 FCRRMAT(19H)
C 1245 FCRRMAT(19H)
C 1250 FCRRMAT(19H)
C 1255 FCRRMAT(19H)
C 1260 FCRRMAT(19H)
C 1265 FCRRMAT(19H)
C 1270 FCRRMAT(19H)
C 1275 FCRRMAT(19H)
C 1280 FCRRMAT(19H)
C 1285 FCRRMAT(19H)
C 1290 FCRRMAT(19H)
C 1295 FCRRMAT(19H)
C 1300 FCRRMAT(19H)
C 1305 FCRRMAT(19H)
C 1310 FCRRMAT(19H)
C 1315 FCRRMAT(19H)
C 1320 FCRRMAT(19H)
C 1325 FCRRMAT(19H)
C 1330 FCRRMAT(19H)
C 1335 FCRRMAT(19H)
C 1340 FCRRMAT(19H)
C 1345 FCRRMAT(19H)
C 1350 FCRRMAT(19H)
C 1355 FCRRMAT(19H)
C 1360 FCRRMAT(19H)
C 1365 FCRRMAT(19H)
C 1370 FCRRMAT(19H)
C 1375 FCRRMAT(19H)
C 1380 FCRRMAT(19H)
C 1385 FCRRMAT(19H)
C 1390 FCRRMAT(19H)
C 1395 FCRRMAT(19H)
C 1400 FCRRMAT(19H)
C 1405 FCRRMAT(19H)
C 1410 FCRRMAT(19H)
C 1415 FCRRMAT(19H)
C 1420 FCRRMAT(19H)
C 1425 FCRRMAT(19H)
C 1430 FCRRMAT(19H)
C 1435 FCRRMAT(19H)
C 1440 FCRRMAT(19H)
C 1445 FCRRMAT(19H)
C 1450 FCRRMAT(19H)
C 1455 FCRRMAT(19H)
C 1460 FCRRMAT(19H)
C 1465 FCRRMAT(19H)
C 1470 FCRRMAT(19H)
C 1475 FCRRMAT(19H)
C 1480 FCRRMAT(19H)
C 1485 FCRRMAT(19H)
C 1490 FCRRMAT(19H)
C 1495 FCRRMAT(19H)
C 1500 FCRRMAT(19H)
C 1505 FCRRMAT(19H)
C 1510 FCRRMAT(19H)
C 1515 FCRRMAT(19H)
C 1520 FCRRMAT(19H)
C 1525 FCRRMAT(19H)
C 1530 FCRRMAT(19H)
C 1535 FCRRMAT(19H)
C 1540 FCRRMAT(19H)
C 1545 FCRRMAT(19H)
C 1550 FCRRMAT(19H)
C 1555 FCRRMAT(19H)
C 1560 FCRRMAT(19H)
C 1565 FCRRMAT(19H)
C 1570 FCRRMAT(19H)
C 1575 FCRRMAT(19H)
C 1580 FCRRMAT(19H)
C 1585 FCRRMAT(19H)
C 1590 FCRRMAT(19H)
C 1595 FCRRMAT(19H)
C 1600 FCRRMAT(19H)
C 1605 FCRRMAT(19H)
C 1610 FCRRMAT(19H)
C 1615 FCRRMAT(19H)
C 1620 FCRRMAT(19H)
C 1625 FCRRMAT(19H)
C 1630 FCRRMAT(19H)
C 1635 FCRRMAT(19H)
C 1640 FCRRMAT(19H)
C 1645 FCRRMAT(19H)
C 1650 FCRRMAT(19H)
C 1655 FCRRMAT(19H)
C 1660 FCRRMAT(19H)
C 1665 FCRRMAT(19H)
C 1670 FCRRMAT(19H)
C 1675 FCRRMAT(19H)
C 1680 FCRRMAT(19H)
C 1685 FCRRMAT(19H)
C 1690 FCRRMAT(19H)
C 1695 FCRRMAT(19H)
C 1700 FCRRMAT(19H)
C 1705 FCRRMAT(19H)
C 1710 FCRRMAT(19H)
C 1715 FCRRMAT(19H)
C 1720 FCRRMAT(19H)
C 1725 FCRRMAT(19H)
C 1730 FCRRMAT(19H)
C 1735 FCRRMAT(19H)
C 1740 FCRRMAT(19H)
C 1745 FCRRMAT(19H)
C 1750 FCRRMAT(19H)
C 1755 FCRRMAT(19H)
C 1760 FCRRMAT(19H)
C 1765 FCRRMAT(19H)
C 1770 FCRRMAT(19H)
C 1775 FCRRMAT(19H)
C 1780 FCRRMAT(19H)
C 1785 FCRRMAT(19H)
C 1790 FCRRMAT(19H)
C 1795 FCRRMAT(19H)
C 1800 FCRRMAT(19H)
C 1805 FCRRMAT(19H)
C 1810 FCRRMAT(19H)
C 1815 FCRRMAT(19H)
C 1820 FCRRMAT(19H)
C 1825 FCRRMAT(19H)
C 1830 FCRRMAT(19H)
C 1835 FCRRMAT(19H)
C 1840 FCRRMAT(19H)
C 1845 FCRRMAT(19H)
C 1850 FCRRMAT(19H)
C 1855 FCRRMAT(19H)
C 1860 FCRRMAT(19H)
C 1865 FCRRMAT(19H)
C 1870 FCRRMAT(19H)
C 1875 FCRRMAT(19H)
C 1880 FCRRMAT(19H)
C 1885 FCRRMAT(19H)
C 1890 FCRRMAT(19H)
C 1895 FCRRMAT(19H)
C 1900 FCRRMAT(19H)
C 1905 FCRRMAT(19H)
C 1910 FCRRMAT(19H)
C 1915 FCRRMAT(19H)
C 1920 FCRRMAT(19H)
C 1925 FCRRMAT(19H)
C 1930 FCRRMAT(19H)
C 1935 FCRRMAT(19H)
C 1940 FCRRMAT(19H)
C 1945 FCRRMAT(19H)
C 1950 FCRRMAT(19H)
C 1955 FCRRMAT(19H)
C 1960 FCRRMAT(19H)
C 1965 FCRRMAT(19H)
C 1970 FCRRMAT(19H)
C 1975 FCRRMAT(19H)
C 1980 FCRRMAT(19H)
C 1985 FCRRMAT(19H)
C 1990 FCRRMAT(19H)
C 1995 FCRRMAT(19H)
C 2000 FCRRMAT(19H)

```


C
 ST02420
 LST02430
 LST02440
 LST02450
 LST02460
 LST02470
 LST02480
 LST02490
 LST02500
 LST02510
 LST02520
 LST02530
 LST02540
 LST02550
 LST02560
 LST02570
 LST02580
 LST02590
 LST02600
 LST02610
 LST02620
 LST02630
 LST02640
 LST02650
 LST02660
 LST02670
 LST02680
 LST02690
 LST02700
 LST02710
 LST02720
 LST02730
 LST02740
 LST02750
 LST02760
 LST02770
 LST02780
 LST02790
 LST02800
 LST02810
 LST02820
 LST02830
 LST02840
 LST02850
 LST02860
 LST02870

```

1  C L J=1,N
2  X(I,J)=1.0
10 DC K=1,N
    DC 3+ L=1,N
    KP=0
11 Z=C
    DC 12 K=L,N
    IF(Z-DABS(A(K,L)))11,12,12
    Z=CABS(A(K,L))
12 KP=X
    CCNTINUE
13 DC 14 J=L,N
    Z=A(L,J)
    A(KP,J)=A(KP,J)
14 DC 15 J=1,N
    Z=X(L,J)
    X(L,J)=X(KP,J)
15 X(KP,J)=Z
    IF(DABS(A(L,L))-EP)50,50,30
20 IF(L-N)31,34,34
21 LPI=L+1
    DC 36 K=LPI,N
    IF(A(K,L))=2,36,32
    IF(A(K,L))/A(L,L)
32 DC 35 J=LPI,N
    A(K,J)=A(K,J)-RATIC*A(L,J)
33 DC 35 J=1,N
    X(K,J)=X(K,J)-RATIC*X(L,J)
35 CCNTINUE
36 DO 43 I=1,N
    CCNTINUE
34 DC 43 I=1,N
    DC 43 J=1,N
    S=C.0
    IF(II-N)41,43,43
    IIP1=I+1
41 DC 42 K=IIP1,N
    S=S+A(IIP1,K)*X(K,J)
42 X(IIP1,J)=(X(IIP1,J)-S)/A(IIP1,II)
43 KER=1
50 KER=2
    RETURN
    END
  
```

LST000010
 LST000020
 LST000030
 LST000040
 LST000050
 LST000060
 LST000070
 LST000080
 LST000090
 LST000100
 LST000110
 LST000120
 LST000130
 LST000140
 LST000150
 LST000160
 LST000170
 LST000180
 LST000190
 LST000200
 LST000210
 LST000220
 LST000230
 LST000240
 LST000250
 LST000260
 LST000270
 LST000280
 LST000290
 LST000300
 LST000310
 LST000320

PER00010
 PER00020
 PER00030
 PER00040
 PER00050
 PER00060
 PER00070
 PER00080
 PER00090
 PER00100
 PER00110
 PER00120

```

REAL FUNCT ION HG*8(AMPL,G,XPN,X,DEL)
IMPLICIT REAL*8 (A-H, O-Z)
DATA CR/0.017453/
TNT = 2.0*XFN-2.0
WRITE(6,991) AMPL,G,XPN,X
FCR MAT(IX,4F10.6)
GS = G**2
TG = 2.0*C*G
OPGS = 1.0+GS
HG = AMPL*(1.0/((1.0-(1.0-G)**(TNT))))-(1.0/((1.0+G)**(TNT))))
1 * (1.0/(OPGS-TG*DCCS(X*CR)**(XPN-1.0))
2 - 1.0/(OPGS-TG*DCCS(X+DEL)*CR)**(XPN-1.0))
WRITE(6,999) AMPL,G,HG,X
FCR MAT(IX,2F10.5,2F10.4,F10.4)
FORMAT(IX,GE,NCF) RETURN
END
REAL FUNCT ION EQN*8(A,X,XB,XC,NCF)
IMPLICIT REAL*8 (A-H, O-Z)
DIMENSION A(10)
GO TO (5,55,155,255), NOF
5 CEL = A(10)
EQN = HG(A(1),A(2),1.5,X,DEL)
RETURN
55 DEL = A(10)
EQN = HG(A(5),A(1),A(2),X,DEL)
RETURN
155 DEL = XB-X
EQN = HG(A(5),A(1),A(2),X,DEL)
RETURN
255 EQN = A(1)*X**2 + A(2)*X + A(3)
RETURN
END
  
```

```

SUBROUTINE PERR(ERRNC,IXS,PARAM,XS,YS,ZS)
INTEGER*4 ERRNO
DIMENSION XS(4), YS(4), ZS(4)
NUP = 4
IF(IXS.LT.4) NUP = IXS
WRITE(6,100) ERRNC,PARAM,IXS
FCR MAT(IXS,ERRNO,DETECTED,LOCATICN NO.,I5,PARAM = ,
14 8,IXS = IIC)
WRITE(6,110) (XS(I),YS(I),ZS(I),I = 1,NUP)
FCR MAT(IXS,COCRD, FROM PERR: ,12F9.5)
RETURN
END
  
```

LIST OF REFERENCES

1. Naval Research Laboratory Report 6152, Experimental Observations of Forward Scattering of Light in the Lower Atmosphere, by J.A. Curcio and L.F. Drummeter, Jr., 30 September 1964.
2. Battelle Memorial Institute Report BAT-171-4, Feasibility of Non-Line-of-Sight Laser Communications, by G.T. Ruck, 15 December 1964.
3. King, M. and Kainer, S., "Some Parameters of a Laser-Type Beyond-the-Horizon Communications Link," Proceedings of the IEEE, v. 53, p. 137-141, February 1965.
4. Naval Electronics Laboratory Center Report 1988 (TR 1988), Extended Line-of-Sight Optical Communications Study, by G.C. Mooradian, V.J. Adrian, P.H. Levine, and W.R. Stone, p. 9, 30 June 1976, changed 4 November 1976.
5. Air Force Cambridge Research Laboratories Report 75-0255, Atmospheric Transmittance from 0.25 to 28.5 μ m: Computer Code LOWTRAN 3, by J.E.A. Selby and R.A. McClatchey, p. 38-44, 7 May 1975.
6. Air Force Cambridge Research Laboratories Report 72-0497, Optical Properties of the Atmosphere, (3rd ed.), by R.A. McClatchey, R.W. Fenn, J.E.A. Selby, F.P. Volz, and J.S. Garing, p. 36-37, 69-71, 24 August 1972.
7. Aeronautical Research Associates of Princeton Report 274, Vol. I, Voice Communication via Scattered Ultraviolet Radiation, by E.S. Fishburne, M.E. Neer, and G. Sandri, February 1976.
8. Aeronautical Research Associates of Princeton Report 285, Voice Communication via Atmospheric Scattering of Ultraviolet Radiation, by E.S. Fishburne and M.E. Neer, July 1976.
9. Bhaumik, M.L., "High Efficiency UV Lasers," Laser Focus, v. 12, p. 55, February 1976.
10. Bhaumik, M.L., Bradford, R.S., Jr., and Ault, E.R., "High Efficiency KrF Eximer Laser," Applied Physics Letters, v. 28, p. 23, 1976.

11. Naval Research Laboratory Memorandum Report 3238, Ultraviolet Extinction Measurements of the Chesapeake Bay, by J.A. Curcio and G.L. Knestrick, p. 12, March 1976.
12. Shettle, E.P. and Green, A.E.S., "Multiple Scattering Calculation of the Middle Ultraviolet Reaching the Ground," Applied Optics, v. 13, p. 1567-1581, July 1974.
13. Stotts, L.B., "The Radiance Produced by Laser Radiation Transversing a Particulate Multiple-Scattering Medium," Journal of the Optical Society of America, v. 67, n. 6, p. 815-819, June 1977.
14. Bucher, E.A., "Computer Simulation of Light Pulse Propagation for Communication Through Thick Clouds," Applied Optics, v. 12, n. 10, p. 2391-2400, October 1973.
15. Bucher, E.A., "Experiments on Light Pulse Communication and Propagation Through Atmospheric Clouds," Applied Optics, v. 12, n. 10, p. 2401-2414, October 1973.
16. Kennedy, R.S., "Communication Through Optical Scattering Channels: An Introduction," Proceedings of the IEEE, v. 58, n. 10, p. 1651-1665, October 1970.
17. Kennedy, E.A., personal communication.
18. Yarif, A., Introduction to Optical Electronics, 2d. ed., Holt, Rinehart and Winston, p. 306-307, 1976.
19. Ault, E.R., Bradford, R.S., Jr., and Bhaumik, M.L., "High-Power Xenon Fluoride Laser," Applied Physics Letters, v. 27, p. 413, 1975.
20. Laser Focus, v. 13, p. 32-33, September 1977.
21. Naval Research Laboratory Report 4031, Horizontal Attenuation of Ultraviolet and Visible Light by the Lower Atmosphere, by L. Dunkelmann, p. 7-10, 13, 17, 19, and 21, 10 September 1952.
22. Penndorf, R., "Tables of the Refractive Index for Standard Air and the Rayleigh Scattering Coefficient for the Spectral Region Between 0.2 and 20.0 μ and Their Application to Atmospheric Optics," Journal of the Optical Society of America, v. 47, n. 2, p. 179, February 1957.

23. Aeronautical Research Associates of Princeton Report 314, Ultraviolet Single Scattering Phase Function of Naturally Occurring Atmospheric Aerosols, by M.E. Neer, J.M. Schlupf, and P.C. Petersen, September 1977.
24. Zachor, A.S., "Aureole Radiance Field About a Source in a Scattering-Absorbing Medium," submitted for publication.
25. Pratt, W.K., Laser Communication Systems, p. 177-178, John Wiley & Sons, Inc., 1969.
26. Ross, M., Laser Receivers, John Wiley & Sons, Inc., 1966.
27. Gagliardi, R.M. and Karp, S., Optical Communications, John Wiley & Sons, 1976.
28. Valley, S.L., Handbook of Geophysics and Space Environments, Air Force Cambridge Research Laboratories, Office of Aerospace Research, U.S. Air Force, p. 7-6, 1965. (Also published by McGraw-Hill Book Co., 1965)
29. Uros, N.M., personal communication.
30. RCA, Electro-Optics Handbook, p. 114-115, 1974.
31. Selby, S.M., Standard Mathematical Tables, 23d ed., p. 103-104, CRC Press, Inc., 1975.
32. Scripps Institution of Oceanography, Reference 71-1, Underwater Lighting by Submerged Lasers and Incandescent Sources, by S.Q. Duntley, June 1971.
33. Duntley, S.Q., Journal of the Optical Society of America, V. 53, p. 214, 1963.

INITIAL DISTRIBUTION LIST

<u>AGENCY</u>	<u>NO. COPIES</u>
1. Defense Documentation Center Cameron Station Alexandria, Virginia 22314	2
2. Dr. Richard S. Hughes Naval Weapons Center China Lake, California	2
3. Dr. Michael E. Neer Aeronautical Research Associates of Princeton, Inc. (ARAP) 50 Washington Road Princeton, New Jersey 08540	1
4. Dr. Alexander S. Zachor Honeywell, Inc. Radiation Center 2 Forbes Road Lexington, Massachusetts 02173	1
5. Associate Professor John P. Powers Code 62Po Department of Electrical Engineering Naval Postgraduate School Monterey, California 93940	1
6. Library, Code 0142 Naval Postgraduate School Monterey, California 93940	2
7. Office of Research Administration Code 012A Naval Postgraduate School Monterey, California 93940	1
8. Department Chairman, Code 61 Department of Physics and Chemistry Naval Postgraduate School Monterey, California 93940	2
9. Professor William M. Tolles, Code 61T1 Department of Physics and Chemistry Naval Postgraduate School Monterey, California 93940	40
10. LT Dennis M. Junge 2705 N. Prospect Colorado Springs, Colorado 80907	2